Optimal DCFP bearing properties and seismic performance assessment in nondimensional form for isolated bridges

OPTIMAL DCFP BEARING PROPERTIES AND SEISMIC PERFORMANCE ASSESSMENT IN NON-DIMENSIONAL FORM FOR ISOLATED BRIDGES

P. Castaldo[1], G. Amendola[2]

[1] Department of Structural, Geotechnical and Building Engineering (DISEG), Politecnico di Torino, Turin, Italy (corresponding author). E-mail: paolo.castaldo@polito.it ; pcastaldo@unisa.it
[2] Department of Structural, Geotechnical and Building Engineering (DISEG), Politecnico di Torino, Turin, Italy. E-mail: guglielmo.amendola@polito.it

SUMMARY

The study analyzes the influence of double concave friction pendulum (DCFP) isolator properties on the seismic performance of isolated multi-span continuous deck bridges. The behaviour of these systems is analyzed by employing an eight-degree-of-freedom model accounting for the pier flexibility in addition to the rigid presence of both abutment and deck, whereas the DCFP isolator behaviour is described combining two single FP devices in series. The uncertainty in the seismic input is taken into account by considering a set of non-frequent natural records with different characteristics. The variation of the statistics of the response parameters relevant to the seismic performance of the isolated bridges is investigated through the proposal of a nondimensionalization of the motion equations, with respect to the seismic intensity, within an extensive parametric study carried out for different isolator and bridge properties. Moreover, two cases related to different ratios between the sliding friction coefficients of the two surfaces of the DCFP devices are analysed with the aim also to evaluate the corresponding optimal values able to minimize the seismic demand to the pier. In this way, all the presented non-dimensional results are useful for the preliminary design or retrofit of multi-span continuous deck bridges, isolated with DCFP devices, located in any site and in relation, especially, to the seismic ultimate limit states.

KEYWORDS: seismic performance, double concave friction pendulum (DCFP) isolator, bridge, non-dimensional form, optimal friction coefficient, limit state.

INTRODUCTION

Seismic isolation has emerged as one of the most powerful techniques in the ensemble of retrofitting methodologies [1]-[5] for infrastructures. In general terms, seismic isolation of bridges permits to obtain the uncoupling of the deck from the horizontal earthquake's components, leading to a significant reduction of the deck acceleration and, as a consequence, of the forces transmitted to the pier. Several researches (e.g., [1]-[4]) have been carried out in the last decades investigating the effectiveness of the isolation devices and carrying out experimental and analytical studies on the seismic response of bridges isolated by sliding isolation systems finding out as these kinds of devices are quite effective in the aseismic bridges' design. Contextually, Ghobarah and Ali [5] together with Turkington et al. [6] showed that the presence of lead-rubber bearings (LRB) shift the natural period of the structure and increases the amount of damping, moreover these devices permit to distribute the seismic forces approximately evenly between pier and abutment. Jangid [7] studied the seismic response of bridges isolated by LRBs to bidirectional earthquakes outlining that the bidirectional interaction of the restoring forces of the LRBs has not negligible effects on the seismic response of the isolated bridges. Closed-form expressions for both the optimum yield strength of LRBs and corresponding response of the isolated bridge system are proposed by [8]. In [9], the effects of soil-structure interaction on the peak responses of three-span continuous deck bridge isolated by the elastomeric bearings have also been evaluated showing their importance in order to not underestimate the bearing displacements at abutment locations. The results of [10] confirm that the isolation can have beneficial effects even for bridges located in medium soil types.
Regarding friction pendulum system (FPS) as isolators, the seismic behaviour of seismically isolated bridges was widely studied by [11]-[14]. In [14], it is illustrated the seismic response analysis of three-span continuous deck bridges isolated with FP bearings and subjected to harmonic motions and real earthquakes. The seismic response of isolated bridges is investigated in [15] confirming the effectiveness of simplified models in relation to the flexibility of the deck and of the piers. Regarding the flexibility of the abutment, a comparative study on seat-type abutment bridges is described in [16], employing real bridges of variable total lengths, openings at the expansion joints and backfill models, through 3D non-linear numerical models to investigate the seismic participation of the abutment and the backfill soil able to reduce effectively the seismic demand of bridges. Similarly, the interaction of the abutment with the backfill soil is widely investigated for integral abutment bridges in [17] as well as the studies by [18]-[19] highlight the importance of considering the soil-structure at the end abutments. When FPS bearings are used, the natural period of the isolated structure becomes independent of the mass of the superstructure and it just has a dependence on the radius of curvature of the sliding surface [20]. Another important feature of this isolation system is mainly related to the energy dissipation mechanism thanks to the velocity-dependent friction between the sliding surfaces and the composite material on the slider [21]-[25]. Eröz and DesRoches [26]-[27] analyzed the effect of modeling parameters and the influence of the design parameters on the response of a three-dimensional multi-span continuous steel girder bridge model seismically isolated

by the FPS. In addition, it has been demonstrated in [28]-[29] that the characteristics of a FPS bearing become more effective by introducing a second sliding surface obtaining the so called double concave friction pendulum (DCFP) device. In particular, Kim and Yun [30] studied the positive effects of a double concave friction pendulum system on a bridge response considering different combinations of radii of curvature and of friction coefficients. Multi-stage performance of seismically isolated bridge using triple pendulum bearings has been investigated in probabilistic terms for different characteristics of the seismic device by [31]. In [32], the optimal properties of the FPS able to minimize the seismic response of pier under earthquakes having different frequency contents representative of different soil conditions is evaluated. In [33], the performance-based evaluation approach through the assessment of the fragility functions is used to investigate the effectiveness and optimum design parameters of isolation (elastomeric and frictional) devices.
Other studies [34]-[38] have been more oriented to define design approaches for the sliding (FPS and DCFP) isolators by means of the seismic reliability-based design (SRBD), in which the main uncertainties such as the seismic input and the system properties have been taken into account. In [39]-[41], specific nondimensionalizations of the motion equations for systems equipped with dampers or sliding isolators are proposed as a function of the structural and earthquake properties. This study analyzes the influence of the double concave friction pendulum isolator properties on the seismic performance of isolated multi-span continuous deck bridges in line with [11],[14],[15]. The behaviour of these structural systems, as also described in [11],[14],[15], is analyzed by employing an eight-degree-of-freedom (8-dof) model representative of the reinforced concrete (RC) pier flexibility, of the DCFP isolators and of the rigid presence of both RC abutment and RC deck. Specifically, the DCFP isolator behaviour is described combining two single FPSs in series [28]-[29] and for each sliding surface, a widespread model which considers the variation of the friction coefficient with the sliding velocity is adopted [23]-[24]. The uncertainty in the seismic input is taken into account by means of a set of non-frequent natural records with different characteristics. The variation of the statistics (i.e., median value and variation) of the response parameters relevant to the seismic performance of isolated bridges is investigated within the proposal of a specific nondimensionalization of the motion equations, as also implemented in [39]-[41] with respect to the seismic intensity. In detail, an extensive non-dimensional parametric study is developed for several structural properties of the pier and of the DCFP isolators monitoring the responses of the deck, of the pier and of each surface of the DCFP isolators. Moreover, two cases related to different ratios between the sliding friction coefficients of the two surfaces of the DCFP devices are analysed. The proposed nondimensionalization motion equations with respect to the seismic intensity has led to perform the parametric analysis achieving non-dimensional results useful for the preliminary design or retrofit of multi-span continuous deck bridges, isolated with DCFP devices, located in any site and in relation, especially, to the seismic ultimate limit states [42] for the kind of ground motions selected. Finally, the optimal normalised values of the sliding friction coefficients for the DCFP isolators able to minimize the seismic demand to the pier are also presented.

SYSTEM DESCRIPTION WITH EQUATIONS OF MOTION

An 8-degree-of-freedom (8-dof) system is employed to model the equivalent configuration for the isolated multi-span continuous deck bridge (e.g., isolated three-span continuous deck bridge) of Fig. 1, analysed also by [11],[14],[15] and representative of real bridges similar to those investigated, for example, in [43]-[44]. Specifically, 5 dof are given by the lumped masses of the elastic RC pier, 2 dof correspond to the two slider masses of the DCFP isolators, located respectively on the elastic RC pier and on the rigid RC abutment, and 1 dof is related to the rigid RC deck mass [11]. The abovementioned model is herein adopted with the purpose to consider the rigid presence of the RC abutment and investigate its influence on the response of the isolators without analysing the possible positive effects deriving from the interaction with the backfill soil, specific for each site, as discussed in [16]-[19]. In fact, considering the only presence of the pier equipped with a DCFP device to isolate the mass deck is effective for a single-column bent viaduct as long as the bridge is straight and consists of a large number of equal spans, of piers with equal height/stiffness and a deck that can be assumed to move as a rigid body [32],[45]. In addition, it is worth underlining that a preliminary analysis has been developed to define the appropriate number of lumped masses to consider the effects of the higher modes, due to the pier flexibility, on the isolator and system performance [32],[43]-[44] for the structural properties assumed next. This 8-dof model is shown in Fig. 1 without any construction details with the aim to illustrate the equivalent discretization useful for the parametric analysis, presented in the next sections. Under these assumptions, the equations of motion governing the response of the model representing a bridge isolated with DCFP isolators, in terms of relative horizontal displacements with respect to the ground (Fig1(a)), subjected to the seismic input $\ddot{u}_g(t)$ along the longitudinal direction, apply:

$$
\begin{aligned}
&m_d\left[\ddot{u}_d(t)+\ddot{u}_g(t)\right]+F_{1a}(t)+F_{1p}(t)=0\\
&m_{sa}\left[\ddot{u}_{sa}(t)+\ddot{u}_g(t)\right]-F_{1a}(t)+F_{2a}(t)=0\\
&m_{sp}\left[\ddot{u}_{sp}(t)+\ddot{u}_g(t)\right]-F_{1p}(t)+F_{2p}(t)=0\\
&m_{p5}\left[\ddot{u}_{p5}(t)+\ddot{u}_g(t)\right]+c_{p5}\left[\dot{u}_{p5}(t)-\dot{u}_{p4}(t)\right]+k_{p5}\left[u_{p5}(t)-u_{p4}(t)\right]-F_{2p}(t)=0\\
&m_{pi}\left[\ddot{u}_{pi}(t)+\ddot{u}_g(t)\right]+c_{pi}\left[\dot{u}_{pi}(t)-\dot{u}_{pi-1}(t)\right]+k_{pi}\left[u_{pi}(t)-u_{pi-1}(t)\right]-c_{pi+1}\left[\dot{u}_{pi+1}(t)-\dot{u}_{pi}(t)\right]-k_{pi+1}\left[u_{pi+1}(t)-u_{pi}(t)\right]=0 \quad for\ \ i=1,\ldots,4
\end{aligned}
\qquad \text{(1a,b,c,d,e)}
$$

where u_d denotes the displacement of the superstructure (i.e., deck) relative to the ground, u_{sp} the displacement of the slider of the DCFP device on the pier with respect to the ground, u_{sa} the displacement of the slider of the DCFP device

on the abutment with respect to the ground, u_{pi} (i=1,..,4,5) the displacement of pier i-th mass relative to the ground, m_d , m_{sp} and m_{sa} the mass of the deck and of the two DCFP devices, respectively, on the pier and on the abutment, m_{pi} (i=1,..,4,5) the i-th lumped mass of the pier, k_{pi} and c_{pi} (i=1,..4,5) respectively the stiffness and inherent viscous damping constant for each dof of the pier, t the time instant, the dot represents differentiation over time, $F_{ja}(t)$ and $F_{jp}(t)$ denote the reactions of the DCFP bearings on the abutment and on the pier, respectively, for the upper (j = *1*) and lower surface (j = *2*). Regarding the reactions of the DCFP bearings, a DCFP device can be modelled as a serial combination of two single FPS isolators. Thus, according to [28]-[29], when the inertial force associated with the movement of the small slider mass can be neglected, the reaction forces at the lower and upper surface (F_2 and F_1) become the same and can be readily obtained as follows:

$$F = F_1 = F_2 = \frac{m_d g}{R_1 + R_2}(u) + \frac{m_d g\left(R_1 \mu_1(\dot{u}_1)\operatorname{sgn}(\dot{u}_1) + R_2 \mu_2(\dot{u}_2)\operatorname{sgn}(\dot{u}_2)\right)}{R_1 + R_2} \tag{2}$$

where u is the global horizontal displacement of the DCFP isolator, u_1 represents the horizontal displacement of the upper surface and u_2 the horizontal displacement of the lower one. The first part of the right hand side of Eq.(2) represents the equivalent restoring stiffness (k_{comb}) of the combined DCFP bearing from which the restoring natural period T_d (or circular frequency ω_d) can be obtained as follows:

$$k_{comb} = \frac{m_d g}{R_1 + R_2} \tag{3}$$

$$T_d = 2\pi\sqrt{(R_1 + R_2)/g} = 2\pi/\omega_d \tag{4}$$

where g is the gravity constant, R_1 and R_2 are, respectively, the upper and lower radius of curvature of the DCFP isolator. In Eq.(2), $\mu_j(\dot{u}_j(t))$, (with j=*1,2*), is the sliding friction coefficient, which depends on the slider slip velocity $\dot{u}_j(t)$ along one of the two bearing internal surfaces and on its sign, $\operatorname{sgn}(\dot{u}_j)$ (for j=*1,2*) with *sgn*(·) denoting the sign function. Note that the subscript "1" always refers to the upper surface, whereas the subscript "2" to the lower surface. On the other hand, the second part of Eq.(2), under the hypothesis that sliding occurs on the both surfaces and in the same direction, represents the equivalent friction coefficient of the DCFP device [28]:

$$\mu_{eqv} = \frac{\mu_1 R_1 + \mu_2 R_2}{R_1 + R_2} \tag{5}$$

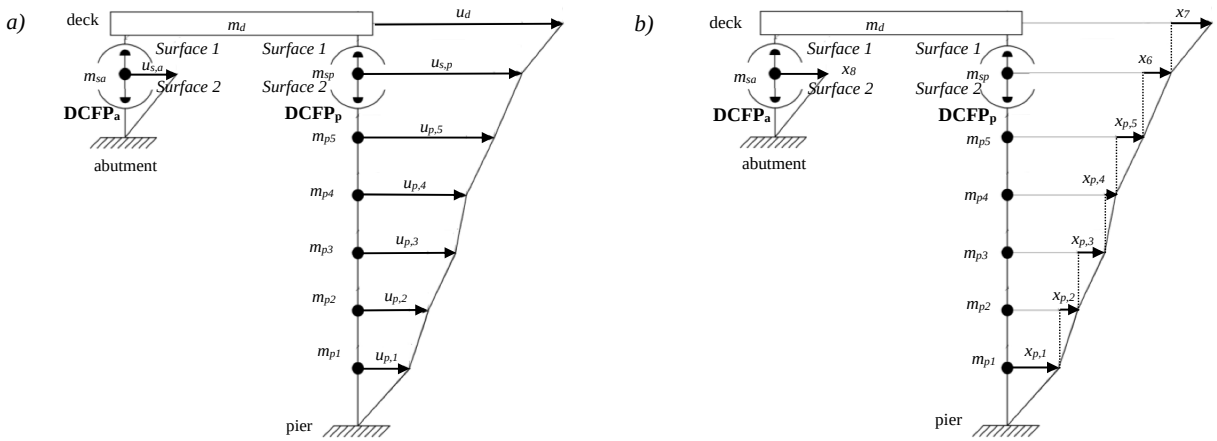

Figure 1. 8-dof model of the bridge isolated with DCFP bearings: relative displacements with respect to the ground (a) and drifts between the lumped masses (b).

In the above discussion, it is also assumed that the DCFP bearings used to isolate the rigid deck, and placed, respectively, on the pier and on the abutment, have the same characteristics, so it is obvious that the two DCFP devices move simultaneously. Moreover, experimental results [22]-[24] suggest that, for each sliding surface, the coefficient of sliding friction of teflon-steel interfaces obeys to the following equation:

$$\mu_j(\dot{u}_j) = \mu_{j,\max} - (\mu_{j,\max} - \mu_{j,\min}) \cdot \exp(-\alpha|\dot{u}_j|) \quad for \quad j = 1,2 \tag{6}$$

in which, referring to the surface j, $\mu_{j,\max}$ represents the maximum value of friction coefficient attained at large sliding velocities and $\mu_{j,\min}$ the value at zero velocity. To further simplify the following analyses, it is assumed that $\mu_{j,\max} = 3\mu_{j,\min}$ based on a regression of the experimental results, whereas the exponent α equal to 30 [22]-[24].

Note that the stiffness contribution of non-structural elements (i.e., kerbs, parapet walls and wearing coat) is neglected. Similarly, the soil-structure interaction and bi-directional or asynchronous effects as well as the vertical component of each ground motion are neglected [11],[14],[15].

PROBLEM FORMULATION AND PROPOSED NON-DIMENSIONALIZATION WITH RESPECT TO THE SEISMIC INTENSITY

In order to analyze the role of each characteristic property controlling the seismic behaviour of the system under investigation, the equations of motion are reduced to a non-dimensional form. The nondimensionalization, herein proposed for the structural configuration of the bridge isolated with DCFP devices, is inspired by the proposals discussed in [40]-[41]. To easily obtain the response of the isolators along each sliding surface, Eq.(1) can be rewritten in terms of drifts between the lumped masses of the system (Fig.1(b)), as follows:

$$
\begin{aligned}
&m_d\ddot{x}_7(t)+m_d\ddot{x}_6(t)+m_d\ddot{x}_{p5}(t)+m_d\ddot{x}_{p4}(t)+m_d\ddot{x}_{p3}(t)+m_d\ddot{x}_{p2}(t)+m_d\ddot{x}_{p1}(t)+F_{1a}(t)+F_{1p}(t)=-m_d\ddot{u}_g(t)\\
&m_{sp}\ddot{x}_6(t)+m_{sp}\ddot{x}_{p5}(t)+m_{sp}\ddot{x}_{p4}(t)+m_{sp}\ddot{x}_{p3}(t)+m_{sp}\ddot{x}_{p2}(t)+m_{sp}\ddot{x}_{p1}(t)-F_{1p}(t)+F_{2p}(t)=-m_{sp}\ddot{u}_g(t)\\
&m_{sa}\ddot{x}_8(t)-F_{1a}(t)+F_{2a}(t)=-m_{sa}\ddot{u}_g(t)\\
&m_{p5}\ddot{x}_{p5}(t)+m_{p5}\ddot{x}_{p4}(t)+m_{p5}\ddot{x}_{p3}(t)+m_{p5}\ddot{x}_{p2}(t)+m_{p5}\ddot{x}_{p1}(t)+c_{p5}\dot{x}_{p5}(t)+k_{p5}x_{p5}(t)-F_{2p}(t)=-m_{p5}\ddot{u}_g(t)\\
&m_{p4}\ddot{x}_{p4}(t)+m_{p4}\ddot{x}_{p3}(t)+m_{p4}\ddot{x}_{p2}(t)+m_{p4}\ddot{x}_{p1}(t)-c_{p5}\dot{x}_{p5}(t)-k_{p5}x_{p5}(t)+c_{p4}\dot{x}_{p4}(t)+k_{p4}x_{p4}(t)=-m_{p4}\ddot{u}_g(t)\\
&m_{p3}\ddot{x}_{p3}(t)+m_{p3}\ddot{x}_{p2}(t)+m_{p3}\ddot{x}_{p1}(t)-c_{p4}\dot{x}_{p4}(t)-k_{p4}x_{p4}(t)+c_{p3}\dot{x}_{p3}(t)+k_{p3}x_{p3}(t)=-m_{p3}\ddot{u}_g(t)\\
&m_{p2}\ddot{x}_{p2}(t)+m_{p2}\ddot{x}_{p1}(t)-c_{p3}\dot{x}_{p3}(t)-k_{p3}x_{p3}(t)+c_{p2}\dot{x}_{p2}(t)+k_{p2}x_{p2}(t)=-m_{p2}\ddot{u}_g(t)\\
&m_{p1}\ddot{x}_{p1}(t)-c_{p2}\dot{x}_{p2}(t)-k_{p2}x_{p2}(t)+c_{p1}\dot{x}_{p1}(t)+k_{p1}x_{p1}(t)=-m_{p1}\ddot{u}_g(t)
\end{aligned}
\qquad (7a,b,c,d,e,f,g,h)
$$

where, according to Eq.s(2)-(6), the reactions of the DCFP bearings, respectively, apply:

$$
F_{1a}=\frac{m_d g}{2}\left[\frac{1}{R_{1a}}\left(\sum_{i=1}^{5}x_{pi}+x_6+x_7-x_8\right)+\mu_{1a}(\dot{x}_9)\left(\operatorname{sgn}(\dot{x}_9)\right)\right],\quad F_{2a}=\left(\frac{m_d}{2}+m_{sa}\right)g\left[\frac{1}{R_{2a}}(x_8)+\left(\mu_{2a}(\dot{x}_8)\right)\left(\operatorname{sgn}(\dot{x}_8)\right)\right]
$$

$$
F_{1p}=\left(\frac{m_d g}{2}\right)\left[\frac{1}{R_{1p}}(x_7)+\left(\mu_{1p}(\dot{x}_7)\right)\left(\operatorname{sgn}(\dot{x}_7)\right)\right],\quad F_{2p}=\left(\frac{m_d}{2}+m_{sp}\right)g\left[\frac{1}{R_{2p}}(x_6)+\left(\mu_{2p}(\dot{x}_6)\right)\left(\operatorname{sgn}(\dot{x}_6)\right)\right]
\qquad (8a,b,c,d)
$$

where $x_9=u_d-x_8=\sum_{i=1}^{5}x_{pi}+x_6+x_7-x_8$. After that, dividing all the equations by m_d, Eq.(7) applies:

$$
\begin{aligned}
&\ddot{x}_7(t)+\ddot{x}_6(t)+\ddot{x}_{p5}(t)+\ddot{x}_{p4}(t)+\ddot{x}_{p3}(t)+\ddot{x}_{p2}(t)+\ddot{x}_{p1}(t)+\\
&+\frac{g}{2}\left[\frac{1}{R_{1a}}\left(\sum_{i=1}^{5}x_{pi}+x_6+x_7-x_8\right)+\mu_{1a}(\dot{x}_9)\left(\operatorname{sgn}\left(\sum_{i=1}^{5}\dot{x}_{pi}+\dot{x}_6+\dot{x}_7-\dot{x}_8\right)\right)\right]+\frac{g}{2}\left[\frac{1}{R_{1p}}(x_7)+\left(\mu_{1p}(\dot{x}_7)\right)\left(\operatorname{sgn}(\dot{x}_7)\right)\right]=\ddot{u}_g(t)
\end{aligned}
$$

$$
\begin{aligned}
&\lambda_{sp}\left(\ddot{x}_6(t)+\ddot{x}_{p5}(t)+\ddot{x}_{p4}(t)+\ddot{x}_{p3}(t)+\ddot{x}_{p2}(t)+\ddot{x}_{p1}(t)\right)+\\
&-\frac{g}{2}\left[\frac{1}{R_{1p}}(x_7)+\left(\mu_{1p}(\dot{x}_7)\right)\left(\operatorname{sgn}(\dot{x}_7)\right)\right]+\left(\frac{1}{2}+\lambda_{sp}\right)g\left[\frac{1}{R_{2p}}(x_6)+\left(\mu_{2p}(\dot{x}_6)\right)\left(\operatorname{sgn}(\dot{x}_6)\right)\right]=-\lambda_{sp}\ddot{u}_g(t)
\end{aligned}
$$

$$
\begin{aligned}
&\lambda_{sa}\ddot{x}_8(t)-\frac{g}{2}\left[\frac{1}{R_{1a}}\left(\sum_{i=1}^{5}x_{pi}+x_6+x_7-x_8\right)+\mu_{1a}(\dot{x}_9)\left(\operatorname{sgn}\left(\sum_{i=1}^{5}\dot{x}_{pi}+\dot{x}_6+\dot{x}_7-\dot{x}_8\right)\right)\right]+\\
&+\left(\frac{1}{2}+\lambda_{sa}\right)g\left[\frac{1}{R_{2a}}(x_8)+\left(\mu_{2a}(\dot{x}_8)\right)\left(\operatorname{sgn}(\dot{x}_8)\right)\right]=-\lambda_{sa}\ddot{u}_g(t)
\end{aligned}
$$

$$
\begin{aligned}
&\lambda_{p5}\left(\ddot{x}_{p5}(t)+\ddot{x}_{p4}(t)+\ddot{x}_{p3}(t)+\ddot{x}_{p2}(t)+\ddot{x}_{p1}(t)\right)+2\xi_{p5}\omega_{p5}\lambda_{p5}\dot{x}_{p5}(t)+\omega_{p5}^2\lambda_{p5}x_{p5}(t)+\\
&-\left(\frac{1}{2}+\lambda_{sp}\right)g\left[\frac{1}{R_{2p}}(x_6)+\left(\mu_{2p}(\dot{x}_6)\right)\left(\operatorname{sgn}(\dot{x}_6)\right)\right]=-\lambda_{p5}\ddot{u}_g(t)
\end{aligned}
$$

$$
\begin{aligned}
&\lambda_{p4}\left(\ddot{x}_{p4}(t)+\ddot{x}_{p3}(t)+\ddot{x}_{p2}(t)+\ddot{x}_{p1}(t)\right)-2\xi_{p5}\omega_{p5}\lambda_{p5}\dot{x}_{p5}(t)-\omega_{p5}^2\lambda_{p5}x_{p5}(t)+2\xi_{p4}\omega_{p4}\lambda_{p4}\dot{x}_{p4}(t)+\omega_{p4}^2\lambda_{p4}x_{p4}(t)=-\lambda_{p4}\ddot{u}_g(t)\\
&\lambda_{p3}\left(\ddot{x}_{p3}(t)+\ddot{x}_{p2}(t)+\ddot{x}_{p1}(t)\right)-2\xi_{p4}\omega_{p4}\lambda_{p4}\dot{x}_{p4}(t)-\omega_{p4}^2\lambda_{p4}x_{p4}(t)+2\xi_{p3}\omega_{p3}\lambda_{p3}\dot{x}_{p3}(t)+\omega_{p3}^2\lambda_{p3}x_{p3}(t)=-\lambda_{p3}\ddot{u}_g(t)\\
&\lambda_{p2}\left(\ddot{x}_{p2}(t)+\ddot{x}_{p1}(t)\right)-2\xi_{p3}\omega_{p3}\lambda_{p3}\dot{x}_{p3}(t)-\omega_{p3}^2\lambda_{p3}x_{p3}(t)+2\xi_{p2}\omega_{p2}\lambda_{p2}\dot{x}_{p2}(t)+\omega_{p2}^2\lambda_{p2}x_{p2}(t)=-\lambda_{p2}\ddot{u}_g(t)\\
&\lambda_{p1}\ddot{x}_{p1}(t)-2\xi_{p2}\omega_{p2}\lambda_{p2}\dot{x}_{p2}(t)-\omega_{p2}^2\lambda_{p2}x_{p2}(t)+2\xi_{p1}\omega_{p1}\lambda_{p1}\dot{x}_{p1}(t)+\omega_{p1}^2\lambda_{p1}x_{p1}(t)=-\lambda_{p1}\ddot{u}_g(t)
\end{aligned}
\qquad (9a,b,c,d,e,f,g,h)
$$

introducing the following ratios:

$$\lambda_{pi}=\frac{m_{pi}}{m_d},\ \lambda_{sa}=\frac{m_{sa}}{m_d},\ \lambda_{sp}=\frac{m_{sp}}{m_d},\ \omega_d=\sqrt{\frac{k_{comb}}{m_d}},\ \omega_{pi}=\sqrt{\frac{k_{pi}}{m_{pi}}},\ \xi_{pi}=\frac{c_{pi}}{2m_{pi}\omega_{pi}}\quad (for\ \ i=1,...,5) \tag{10a,b,c,d,e,f}$$

where the first three terms are the mass ratios, the third and the fourth terms are the circular frequency of vibration of the isolated deck and of the *i*-th dof of the pier and the last one denotes the damping factor of the *i*-th dof of the pier.

Inspired from [40]-[41], let us introduce the time scale $\tau=t\omega_d$, in which ω_d is the fundamental circular frequency of the isolated system (Eq.(4)) with infinitely rigid superstructure considering the stiffness of the DCFP isolator k_{comb} (Eq.(3)), and the seismic intensity scale a_0, expressed as $\ddot{u}_g(t)=a_0\ell(\tau)$ where $\ell(\tau)$ is a non-dimensional function of time describing the seismic input time-history. In this way, applying the abovementioned scaling transformations to the non differential and to the first and second order differential terms of Eq.s(7)-(9), from the parameters $x_{p1}(t),\ x_{p2}(t),x_{p3}(t),x_{p4}(t),x_{p5}(t),x_6(t),x_7(t),x_8(t),x_9(t)$, the following non-dimensional parameters, respectively, derive

$\psi_{p1}(\tau),\ \psi_{p2}(\tau),\psi_{p3}(\tau),\psi_{p4}(\tau),\psi_{p5}(\tau),\psi_6(\tau),\psi_7(\tau),\psi_8(\tau),\psi_9(\tau)$ where $\psi_{p_i}=\frac{x_{pi}\omega_d^2}{a_0}$ for *i*=1,...,5 and $\psi_i=\frac{x_i\omega_d^2}{a_0}$ for *i*=6,...,9. Also defining, consequently, the corresponding non-dimensional first and second order differential terms, from Eq.(9), the following non-dimensional equations (i.e., normalised with respect to the seismic intensity) can be proposed:

$$\ddot{\psi}_7(\tau)+\ddot{\psi}_6(\tau)+\ddot{\psi}_{p5}(\tau)+\ddot{\psi}_{p4}(\tau)+\ddot{\psi}_{p3}(\tau)+\ddot{\psi}_{p2}(\tau)+\ddot{\psi}_{p1}(\tau)+\frac{g}{2}\left[\frac{1}{R_{1p}}\frac{1}{\omega_d^{\,2}}\psi_7(\tau)+\frac{\mu_{1p}(\dot{\psi}_7)}{a_0}\mathrm{sgn}(\dot{\psi}_7)\right]+$$
$$+\frac{g}{2}\left[\frac{1}{R_{1a}}\frac{1}{\omega_d^{\,2}}\left(\sum_{i=1}^{5}\psi_{pi}(\tau)+\psi_6(\tau)+\psi_7(\tau)-\psi_8(\tau)\right)+\left(\frac{\mu_{1a}(\dot{\psi}_9)}{a_0}\right)\left(\mathrm{sgn}\left(\sum_{i=1}^{5}\dot{\psi}_{pi}(\tau)+\dot{\psi}_6(\tau)+\dot{\psi}_7(\tau)-\dot{\psi}_8(\tau)\right)\right)\right]=-\ell(\tau)$$

$$\lambda_{sp}\left[\ddot{\psi}_6(\tau)+\ddot{\psi}_{p5}(\tau)+\ddot{\psi}_{p4}(\tau)+\ddot{\psi}_{p3}(\tau)+\ddot{\psi}_{p2}(\tau)+\ddot{\psi}_{p1}(\tau)\right]-\frac{g}{2}\left[\frac{1}{R_{1p}}\frac{1}{\omega_d^{\,2}}\psi_7(\tau)+\frac{\mu_{1p}(\dot{\psi}_7)}{a_0}\mathrm{sgn}(\dot{\psi}_7)\right]+$$
$$+\left(\frac{1}{2}+\lambda_{sp}\right)g\left[\frac{1}{R_{2p}}\frac{1}{\omega_d^{\,2}}\psi_6(\tau)+\frac{\mu_{2p}(\dot{\psi}_6)}{a_0}\mathrm{sgn}(\dot{\psi}_6)\right]=-\lambda_{sp}\ell(\tau)$$

$$\lambda_{sa}\ddot{\psi}_8(\tau)-\frac{g}{2}\left[\frac{1}{R_{1a}}\frac{1}{\omega_d^{\,2}}\left(\sum_{i=1}^{5}\psi_{pi}(\tau)+\psi_6(\tau)+\psi_7(\tau)-\psi_8(\tau)\right)+\left(\frac{\mu_{1a}(\dot{\psi}_9)}{a_0}\right)\left(\mathrm{sgn}\left(\sum_{i=1}^{5}\dot{\psi}_{pi}(\tau)+\dot{\psi}_6(\tau)+\dot{\psi}_7(\tau)-\dot{\psi}_8(\tau)\right)\right)\right]+$$
$$+\left(\frac{1}{2}+\lambda_{sa}\right)g\left[\frac{1}{R_{2a}}\frac{1}{\omega_d^{\,2}}\psi_8(\tau)+\frac{\mu_{2a}(\dot{\psi}_8)}{a_0}\mathrm{sgn}(\dot{\psi}_8)\right]=-\lambda_{sa}\ell(\tau)$$

$$\lambda_{p5}\left[\ddot{\psi}_{p5}(\tau)+\ddot{\psi}_{p4}(\tau)+\ddot{\psi}_{p3}(\tau)+\ddot{\psi}_{p2}(\tau)+\ddot{\psi}_{p1}(\tau)\right]+2\xi_{p5}\lambda_{p5}\frac{\omega_{p5}}{\omega_d}\dot{\psi}_{p5}(\tau)+\frac{\lambda_{p5}\omega_{p5}^2}{\omega_d^2}\psi_{p5}(\tau)+$$
$$-\left(\frac{1}{2}+\lambda_{sp}\right)g\left[\frac{1}{R_{2p}}\frac{1}{\omega_d^{\,2}}\psi_6(\tau)+\frac{\mu_{2p}(\dot{\psi}_6)}{a_0}\mathrm{sgn}(\dot{\psi}_6)\right]=-\lambda_{p5}\ell(\tau)$$

$$\lambda_{p4}\left[\ddot{\psi}_{p4}(\tau)+\ddot{\psi}_{p3}(\tau)+\ddot{\psi}_{p2}(\tau)+\ddot{\psi}_{p1}(\tau)\right]-2\xi_{p5}\lambda_{p5}\frac{\omega_{p5}}{\omega_d}\dot{\psi}_{p5}(\tau)+2\xi_{p4}\lambda_{p4}\frac{\omega_{p4}}{\omega_d}\dot{\psi}_{p4}(\tau)-\lambda_{p5}\frac{\omega_{p5}^2}{\omega_d^2}\psi_{p5}(\tau)+\lambda_{p4}\frac{\omega_{p4}^2}{\omega_d^2}\psi_{p4}(\tau)=-\lambda_{p4}\ell(\tau)$$
$$\lambda_{p3}\left[\ddot{\psi}_{p3}(\tau)+\ddot{\psi}_{p2}(\tau)+\ddot{\psi}_{p1}(\tau)\right]-2\xi_{p4}\lambda_{p4}\frac{\omega_{p4}}{\omega_d}\dot{\psi}_{p4}(\tau)+2\xi_{p3}\lambda_{p3}\frac{\omega_{p3}}{\omega_d}\dot{\psi}_{p3}(\tau)-\lambda_{p4}\frac{\omega_{p4}^2}{\omega_d^2}\psi_{p4}(\tau)+\lambda_{p3}\frac{\omega_{p3}^2}{\omega_d^2}\psi_{p3}(\tau)=-\lambda_{p3}\ell(\tau)$$
$$\lambda_{p2}\left[\ddot{\psi}_{p2}(\tau)+\ddot{\psi}_{p1}(\tau)\right]-2\xi_{p3}\lambda_{p3}\frac{\omega_{p3}}{\omega_d}\dot{\psi}_{p3}(\tau)+2\xi_{p2}\lambda_{p2}\frac{\omega_{p2}}{\omega_d}\dot{\psi}_{p2}(\tau)-\lambda_{p3}\frac{\omega_{p3}^2}{\omega_d^2}\psi_{p3}(\tau)+\lambda_{p2}\frac{\omega_{p2}^2}{\omega_d^2}\psi_{p2}(\tau)=-\lambda_{p2}\ell(\tau)$$
$$\lambda_{p1}\ddot{\psi}_{p1}(\tau)-2\xi_{p2}\lambda_{p2}\frac{\omega_{p2}}{\omega_d}\dot{\psi}_{p2}(\tau)+2\xi_{p1}\lambda_{p1}\frac{\omega_{p1}}{\omega_d}\dot{\psi}_{p1}(\tau)-\lambda_{p2}\frac{\omega_{p2}^2}{\omega_d^2}\psi_{p2}(\tau)+\lambda_{p1}\frac{\omega_{p1}^2}{\omega_d^2}\psi_{p1}(\tau)=-\lambda_{p1}\ell(\tau)$$

(11a,b,c,d,e,f,g,h)

It derives that the following non-dimensional parameters controlling the bridge system of Figure 1 are obtained:

$$\Pi_{\omega i}=\frac{\omega_{pi}}{\omega_d}\ ,\ \Pi_{\lambda i}=\lambda_{pi}=\frac{m_{pi}}{m_d}\ ,\ \Pi_{\lambda sa}=\lambda_{sa}\ ,\ \Pi_{\lambda sp}=\lambda_{sp}\ ,\ \Pi_{\mu 1a}(\dot{\psi}_9)=\frac{\mu_{1a}(\dot{\psi}_9)g}{a_0}\ ,$$
$$\Pi_{\mu 1p}(\dot{\psi}_7)=\frac{\mu_{1p}(\dot{\psi}_7)g}{a_0}\ ,\ \Pi_{\mu 2a}(\dot{\psi}_8)=\frac{\mu_{2a}(\dot{\psi}_8)g}{a_0}\ ,\ \Pi_{\mu 2p}(\dot{\psi}_6)=\frac{\mu_{2p}(\dot{\psi}_6)g}{a_0}\ ,\ \Pi_{\xi_{pi}}=\xi_{pi}\quad (for\ \ i=1,...,5)$$

(12a,b,c,d,e,f,g,h,i)

$\Pi_{\lambda i,}\ \Pi_{\lambda sa,}\ \Pi_{\lambda sp}$ correspond to the previously defined mass ratios, $\Pi_{\xi_{pi}}$ describes the viscous damping inherent related to the pier *i*-th dof. Regarding the control parameters of the pier, indeed, the parameters ω_{pi} are related to the fundamental vibration pulsation ω_p (the first vibration mode) as well as the sum of the mass ratios is related to the overall mass ratio $\Pi_\lambda = \lambda_p = \sum_{i=1,5} m_{pi} / m_d$ and, finally, all the damping factors $\Pi_{\xi_{pi}}$ can be assumed equal to $\Pi_{\xi_p} = \xi_p$. The non-dimensional or normalized parameters $\Pi_{\mu 1a}$, $\Pi_{\mu 1p}$, $\Pi_{\mu 2a}$, $\Pi_{\mu 2p}$ measure, respectively, the isolator strengths, provided by the friction coefficients of the two surfaces of the two DCFP isolators. Since these parameters depend on the response through the velocities, each one is used in its stead as follows:

$$\Pi^*_{\mu 1a} = \frac{\mu_{1,\max,a} g}{a_0},\ \ \Pi^*_{\mu 1p} = \frac{\mu_{1,\max,p} g}{a_0},\ \ \Pi^*_{\mu 2a} = \frac{\mu_{2,\max,a} g}{a_0},\ \ \Pi^*_{\mu 2p} = \frac{\mu_{2,\max,p} g}{a_0} \qquad (13a,b,c,d)$$

It is important to observe that the normalized response of the dynamic system does not depend on the seismic intensity level a_0. Conversely, the seismic response depends on the function $\ell(\tau)$ and also on the isolation circular frequency ω_d (or period $T_d = 2\pi / \omega_d$ of Eq.(4)). Referring to Fig. 1 and in line with the non-dimensional (or normalized) terms of Eq.(11), it also derives that the non-dimensional peak response parameters describing the peak dynamic response of the deck, of the pier and of the two sliding surfaces of the two DCFP bearings can be defined, respectively, as follows:

$$\psi_{u_d} = \frac{u_{d,\text{peak}}\omega_d^2}{a_0} = \frac{(x_8 + x_9)_{\text{peak}}\omega_d^2}{a_0},\ \ \psi_{x_d} = \frac{x_{d,\text{peak}}\omega_d^2}{a_0} = \frac{(x_6 + x_7)_{\text{peak}}\omega_d^2}{a_0},\ \ \psi_{u_p} = \frac{u_{p,\text{peak}}\omega_d^2}{a_0} = \frac{\left(\sum_{i=1}^{5} x_i\right)_{\text{peak}}\omega_d^2}{a_0}, \qquad (14a,b,c,d,e,f,g)$$

$$\psi_{x_6} = \frac{x_{6,\text{peak}}\omega_d^2}{a_0},\quad \psi_{x_7} = \frac{x_{7,\text{peak}}\omega_d^2}{a_0},\quad \psi_{x_8} = \frac{x_{8,\text{peak}}\omega_d^2}{a_0},\quad \psi_{x_9} = \frac{(u_d - x_8)_{\text{peak}}\omega_d^2}{a_0}$$

Known the structural properties and the seismic intensity level, Eq.s(13a-d) and Eq.s(14a-g) are linear expressions which relate the values in non-dimensional (or normalised) form to those in dimensional (or non-normalised) form, respectively, for the friction coefficients of the two DCFP devices surfaces and for the relevant response parameters.

The proposed nondimensionalization of the motion equations with respect to the seismic intensity and specialized for bridges isolated with DCFP devices have led to equations (Eq.(11)) with parameters defined in a new time domain and independent on the seismic intensity. This means that the following results, in non-dimensional form, can be useful for the preliminary design or retrofit of multi-span continuous deck bridges, isolated with DCFP devices, located in any site and in relation, especially, to the seismic ultimate limit states if non-frequent ground motions are employed, as specified in the next section.

PARAMETRIC STUDY

This section presents the non-dimensional results of an extensive parametric study carried out on the bridge system of Fig 1 to evaluate the seismic performance of bridges isolated with DCFP bearings. The first two subsections describe, respectively, the selection of the earthquake events and the response parameters used to monitor the seismic performance; the final subsection discusses the parametric study results in non-dimensional form also comparing the outcomes of two cases corresponding to different ratios between the sliding friction coefficients of the two surfaces of the DCFP isolators.

Seismic intensity and ground motions

The evaluation of the seismic performance of any engineered system should account for the variability of the intensity, frequency content and duration of the records at the site. Coherently with the performance-based earthquake engineering (PBEE) approach [46]-[47], this study separates the uncertainties related to the seismic input intensity from those on the characteristics of the record (i.e., record-to-record variability) by introducing an intensity measure *IM* that corresponds to the scale factor, a_0 , introduced in the proposed nondimensionalization (i.e., *IM*= a_0) (Eq.(11)). By this way, the randomness in the seismic intensity is described by a hazard curve, whereas the ground motion randomness for a fixed seismic intensity level is described by selecting a set of ground motions characterized by a different duration and frequency content, and by scaling these records to the common a_0 value. In line with the criteria of efficiency, sufficiency and hazard computability [48]-[49], in this study, the spectral pseudo-acceleration, S_A , at the isolated period of the system, $T_d = 2\pi / \omega_d$ (Eq.(4)), is assumed as intensity measure. Many studies (e.g., [48]-[49]) showed that S_A is more efficient than the peak ground acceleration, and its use permits to reduce the response dispersion for the same number of ground motions considered and to obtain more confident response estimates for a given number of records employed. As deducible from all the equations, previously presented, the inherent damping factor of the DCFS devices (consequently also of the deck) is assumed equal to zero, consistently with [12],[41],[57]. Therefore, the corresponding *IM*= a_0 is hereinafter denoted to as $S_A(T_d)$. Furthermore, the choice of $S_A(T_d)$ as *IM*= a_0 is also justified by the fact that if all

the records are normalized to $S_A(T_d)$, then the normalized displacement response of a rigid deck with an isolated period T_d, mounted on a frictionless isolator and on an infinitely stiff pier, is equal to 1 without any influence due to the record-to-record variability. Thus, this system represents a reference case.
The record-to-record variability is herein described through a set of 30 non-frequent real ground motion records with moment magnitude between 6 and 7.6. More details may be found in [35]-[37]. The selection of the real ground motions has not been carried out in line with the conditional spectra criteria, very useful for reliability analysis as widely commented in [50]-[55]. Since the aim of the present study is to propose a nondimensionalization of the motion equations with respect to the seismic intensity in order to provide useful recommendations for isolated bridges in any site and in relation, especially, to the seismic ultimate limit states (i.e., "life safety" and "collapse prevention") [42], a set of non-frequent strong motions has been adopted [35]-[37]. These strong motions have been selected to reproduce quite well both the record-to-record variability (i.e., 30 records) and event-to-event variability (i.e., 19 different earthquake events) [35]-[37], also in line with [56].

Seismic performance in terms of relevant non-dimensional response parameters

This study considers the following peak response parameters relevant to assess the performance of the isolated bridge system of Fig. 1 according to Eq.(14): the peak deck response $u_{d,\text{peak}}$ that coincides with the peak isolator global response on the abutment, the peak isolator global response on the pier $x_{d,\text{peak}}$, the peak displacement at the top of the pier with respect to the ground $u_{p,\text{peak}}$, the peak isolator response along each surface: $x_{6,\text{peak}}$ and $x_{7,\text{peak}}$ respectively for the lower and upper surface of the DCFP device on the pier; $x_{8,\text{peak}}$ and $x_{9,\text{peak}}$ respectively for the lower and upper surface of the DCFP device on the abutment. These peak response parameters have been expressed in non-dimensional form according to Eq.s (11) and (14). By repeatedly solving Eq. (11) for the ground motions records, a set of samples is obtained for each output variable used to monitor the seismic performance of the isolated bridge. In this paper, the non-dimensional response parameters are assumed to follow a lognormal distribution as widely employed in PBEE [47] and in many studies [34]-[38],[57]-[58]. The lognormality assumption permits to estimate, with a limited number of samples, the response at different percentiles, useful also to evaluate the seismic risk [59]. A lognormal distribution can be fitted to the generic non-dimensional response parameter D (i.e., the extreme values of ψ_{u_d}, ψ_{x_d}, ψ_{u_p}, ψ_{x_i} of Eq.s (11) and (14)) by estimating the sample geometric mean, $GM(D)$, and the sample dispersion, $\beta(D)$, defined, respectively, as follows:

$$GM(D) = \sqrt[N]{d_1 \cdot \ldots \cdot d_N} \tag{15}$$

$$\beta(D) = \sigma_{\ln}(D) = \sqrt{\frac{\left(\ln d_1 - \ln\left[GM(D)\right]\right)^2 + \ldots\ldots + \left(\ln d_N - \ln\left[GM(D)\right]\right)^2}{N-1}} \tag{16}$$

where d_h denotes the h-th sample value of D, related to the h-th accelerogram and N is the total number of samples (i.e., total number of accelerograms in this study): h=1,…,N. The sample geometric mean is an estimator of the median of the response and its logarithm coincides with the lognormal sample mean $\mu_{\ln}(D)$. For small values, e.g., below 0.3, the dispersion $\beta(D)$ is approximately equal to the coefficient of variation of the distribution [59]. Under the lognormality assumption, the relation between the geometric mean $GM(D)$, the dispersion $\beta(D)$, and the k-th percentile of the generic response parameter D can be expressed as:

$$d_k = GM(D)\exp[f(k)\beta(D)] \tag{17}$$

where $f(k)$ is a function assuming the values $f(50) = 0$ and $f(84) = 1$ [60].

Results of the non-dimensional parametric study

This section shows the results of the parametric study carried out through the proposed nondimensionalization (Section 3) to evaluate the influence of the isolation devices and bridge properties on the seismic performance of the structural system under the selected ground motions. The parameter $\Pi_{\xi_p} = \xi_p$ is assumed equal to 5%, the isolated bridge period T_d is varied in the range between 2s, 2.5s, 3s, 3.5s and 4s, the RC elastic pier period T_p in the range between 0.05s, 0.1s, 0.15s and 0.2s, typical values in line with [28],[30],[62]-[65]. Assuming that the five pier lumped masses are equal, $\Pi_\lambda = \lambda_p$ has been considered varying in the range between 0.1, 0.15 and 0.2 [30],[62]-[65]. The two DCFP devices on the abutment and on the pier are identical. So, it follows that $\Pi^*_{\mu 1a} = \Pi^*_{\mu 1p} = \Pi^*_{\mu 1}$ as well as $\Pi_{\lambda sa} = \Pi_{\lambda sp} = \Pi_{\lambda s}$. For numerical reasons, the mass ratio $\Pi_{\lambda s}$ is set equal to 0.005. The parameter $\Pi^*_{\mu 1}$ is assumed to vary in the range between 0 (no friction) and 2 (very high friction). In addition, two cases for the DCFP bearings properties have been assumed [28],[30] as listed in Table 1: two different ratios between the sliding friction coefficient of the upper surface with respect

to the one of the lower surface are herein considered for both the abutment's isolator and pier's isolator. Therefore, the non-dimensional numerical investigations have been carried out on 5700 different systems, defined by varying the main structural properties within the two bearing cases, subjected to the 30 different ground motions.

Table 1. DCFP bearings properties within the non-dimensional parametric analysis [28],[30].

	R_1 / R_2	$\mu_{1,\max} / \mu_{2,\max}$	$\mu_{j,\max} / \mu_{j,\min}$ (with $j=1,2$)
case 1	2	4	3
case 2	2	2	3

For each value of the parameters of interest in the parametric study, the differential equations of motion, (i.e., Eq. (11)), have been repeatedly solved for the different ground motions considered. The Bogacki-Shampine integration algorithm available in Matlab-Simulink [61] has been employed choosing a variable step to improve the solution accuracy. The probabilistic properties of the normalized response parameters of interest have been evaluated by estimating the geometric mean, *GM*, and the dispersion, β, through Eq.s (15) and (16). Fig.s 2-8 show the *GM* and β values of the non-dimensional peak response parameters considered, obtained for different values of the system properties varying in the range of interest and related to the case 1 of Table 1. Only the results for T_p= 0.1s and T_p= 0.2s are reported due to space constraints.
Fig. 2 plots the results concerning the peak normalized displacement of pier top ψ_{u_p} with respect to the ground for the case 1. It is noteworthy that for very low $\Pi^*_{\mu 1}$ values, $GM\left(\psi_{u_p}\right)$ decreases by increasing $\Pi^*_{\mu 1}$, whereas it increases for high $\Pi^*_{\mu 1}$ values. Thus, there exists an optimal value of $\Pi^*_{\mu 1}$ such that the peak displacement of pier top is minimized. This optimal value varies between 0 and 0.5 depending on the values of T_d, T_p and Π_λ. In addition, $GM\left(\psi_{u_p}\right)$ decreases significantly with increasing Π_λ and decreasing T_p, which controls directly the main mode of the pier (for higher ω_d^2, smaller will be the displacement of the pier top). T_d has an influence on $GM\left(\psi_{u_p}\right)$ leading to a general decrease for an its increase thanks to the effectiveness of the seismic isolation. The dispersion $\beta\left(\psi_{u_p}\right)$ shows a maximum value approximately at the same value of $\Pi^*_{\mu 1}$ that gives the minimum $GM\left(\psi_{u_p}\right)$. The response dispersion increases with increasing the vibration period T_p and mass ratio Π_λ. From low to high values of T_d, $\beta\left(\psi_{u_p}\right)$ also increases.

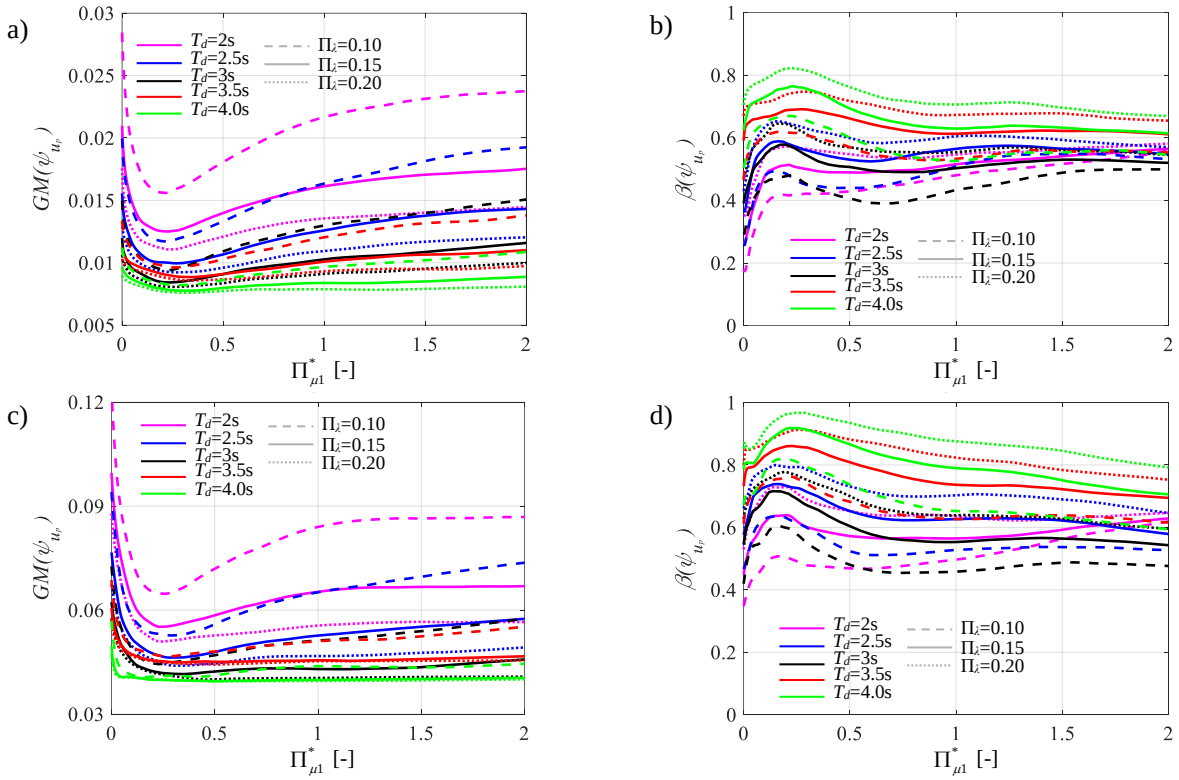

Figure 2. Normalized displacement of pier top vs. $\Pi^*_{\mu 1}$: median value and dispersion for T_p = 0.1s (a and b) and T_p = 0.2s (c and d), for different values of Π_λ and T_d. Case 1.

Within the case 1, Fig.s 3 (a) and (c) show the response statistics of the peak normalized deck displacement ψ_{u_d}, which also corresponds to the peak global response of the bearing placed on the abutment. Obviously, $GM\left(\psi_{u_d}\right)$ decreases significantly as $\Pi^*_{\mu 1}$ increases. In general, the values of $GM\left(\psi_{u_d}\right)$ slightly increase for increasing values of T_d and decreasing values of Π_λ, and are not significantly affected by T_p. The values of the dispersion $\beta\left(\psi_{u_d}\right)$, plotted in Fig.s 3 (b) and (d), are very low for low $\Pi^*_{\mu 1}$ values due to the high efficiency of the *IM*, and attain their maximum for high values of $\Pi^*_{\mu 1}$. The other system properties have a reduced influence on $\beta\left(\psi_{u_d}\right)$ compared to the influence of $\Pi^*_{\mu 1}$.
As for the case 1, Fig.s 4 (a) and (c) show the variation of the peak normalized global response with regard to the bearing placed on the pier ψ_{x_d}. As already observed for $GM\left(\psi_{u_d}\right)$, also $GM\left(\psi_{x_d}\right)$ tends to show a decrease against increasing $\Pi^*_{\mu 1}$ values. The dispersion is low in correspondence of low $\Pi^*_{\mu 1}$ values due to the high efficiency of the *IM*, attaining its peak for high $\Pi^*_{\mu 1}$ values. Note that the influence of both Π_λ and T_p is slightly more marked for $GM\left(\psi_{x_d}\right)$ with respect to $GM\left(\psi_{u_d}\right)$ leading to lower values due to the flexibility of the pier.
Fig.s 5 (a) and (c) show the variation with the system properties of the geometric mean of the peak normalized pier bearing response along the lower surface (surface 2) $GM(\psi_{x_6})$, for T_p = 0.1s and T_p = 0.2s, with regard to the case 1. This sliding surface is characterised by lower values of both radius of curvature and sliding friction coefficient (Table 1). $GM(\psi_{x_6})$ decreases at first quickly, and then slightly increases for values of $\Pi^*_{\mu 1}$ higher than 0.5 and, successively, tends to slightly decrease again. It increases for increasing T_d. The values of the dispersion $\beta\left(\psi_{x_6}\right)$, plotted in Figs. 5 (b) and (d), are very low for low $\Pi^*_{\mu 1}$ values due to the high efficiency of the *IM*, and increase quite monotonically with $\Pi^*_{\mu 1}$. The other system properties have again a negligible influence on $\beta\left(\psi_{x_6}\right)$ in comparison to the influence of $\Pi^*_{\mu 1}$.

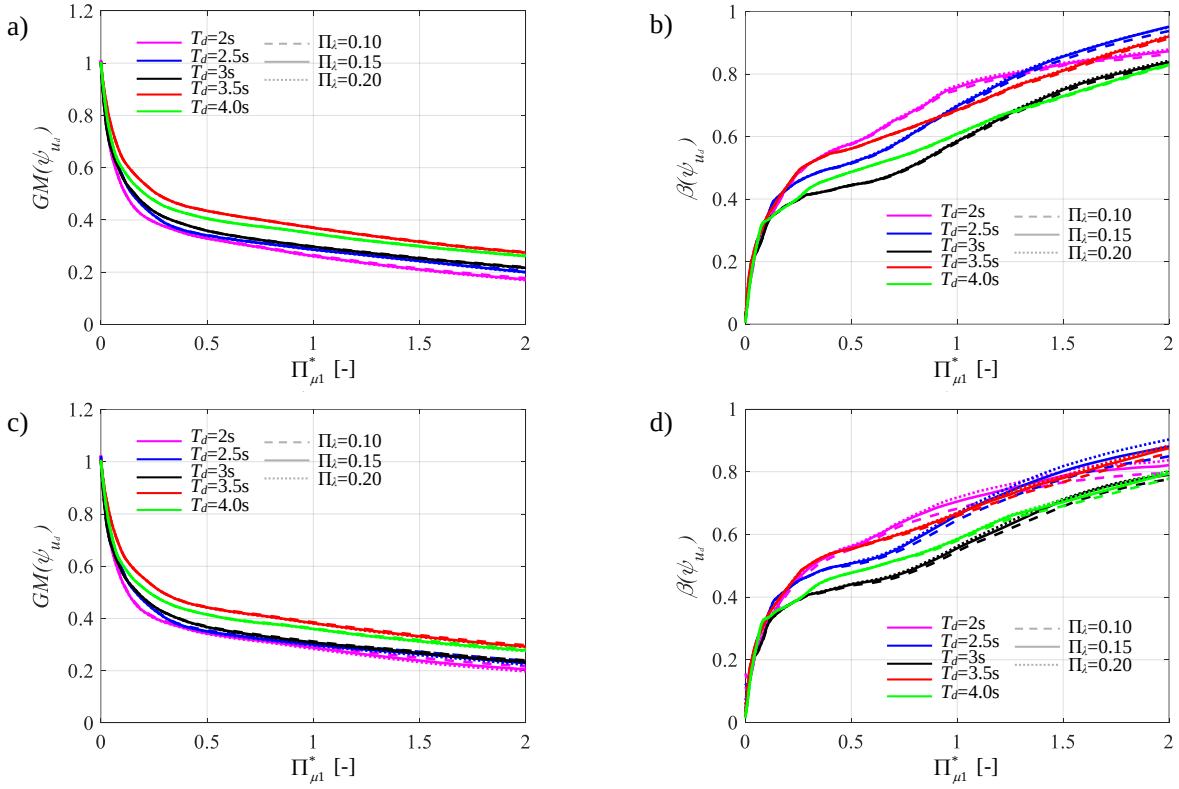

Figure 3. Normalized deck displacement vs. $\Pi^*_{\mu 1}$: median value and dispersion for T_p = 0.1s (a and b) and T_p = 0.2s (c and d), for different values of Π_λ and T_d. Case 1.

Fig.s 6 (a) and (c) show the variation with the system properties of the geometric mean of the peak normalized pier bearing response along the upper surface (surface 1) $GM(\psi_{x_7})$, for T_p = 0.1s and T_p = 0.2s, with regard to the case 1. This sliding surface is characterised by higher values of both radius of curvature and sliding friction coefficient (Table 1). $GM(\psi_{x_7})$

hyperbolically decreases with increasing $\Pi^*_{\mu 1}$. The values of the dispersion $\beta\left(\psi_{x_7}\right)$, plotted in Fig.s 6 (b) and (d), are very low for low $\Pi^*_{\mu 1}$ values due to the efficiency of the *IM*, and show high values for $\Pi^*_{\mu 1}$ in the range 1 - 1.5. It shows an increase against increasing values of T_d. Once again, the other system properties such as T_p and Π_λ have no a significant influence on $\beta\left(\psi_{x_7}\right)$ compared to the influence of $\Pi^*_{\mu 1}$.

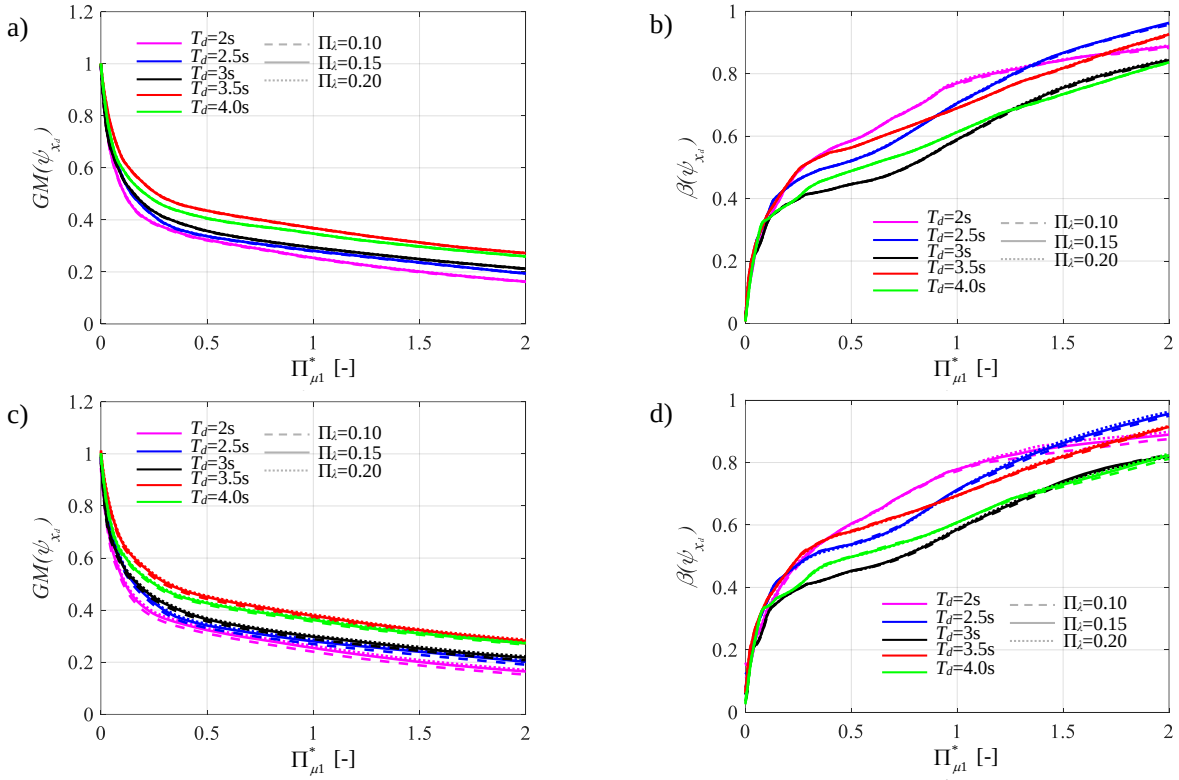

Figure 4. Normalized pier bearing global displacement vs. $\Pi^*_{\mu 1}$: median value and dispersion for T_p = 0.1s (a and b) and T_p = 0.2s (c and d), for different values of Π_λ and T_d. Case 1.

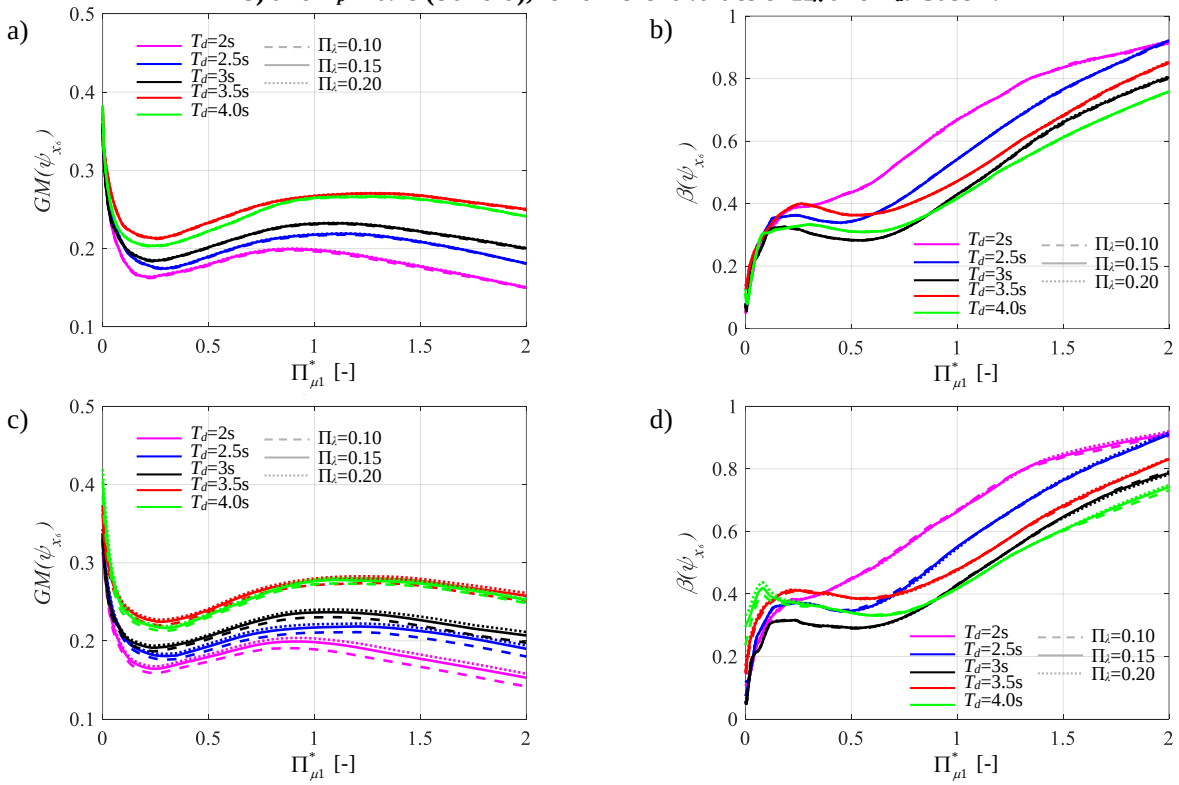

Figure 5. Normalized pier bearing response along the lower surface vs. $\Pi^*_{\mu 1}$: median value and dispersion for T_p = 0.1s (a and b) and T_p = 0.2s (c and d), for different values of Π_λ and T_d. Case 1.

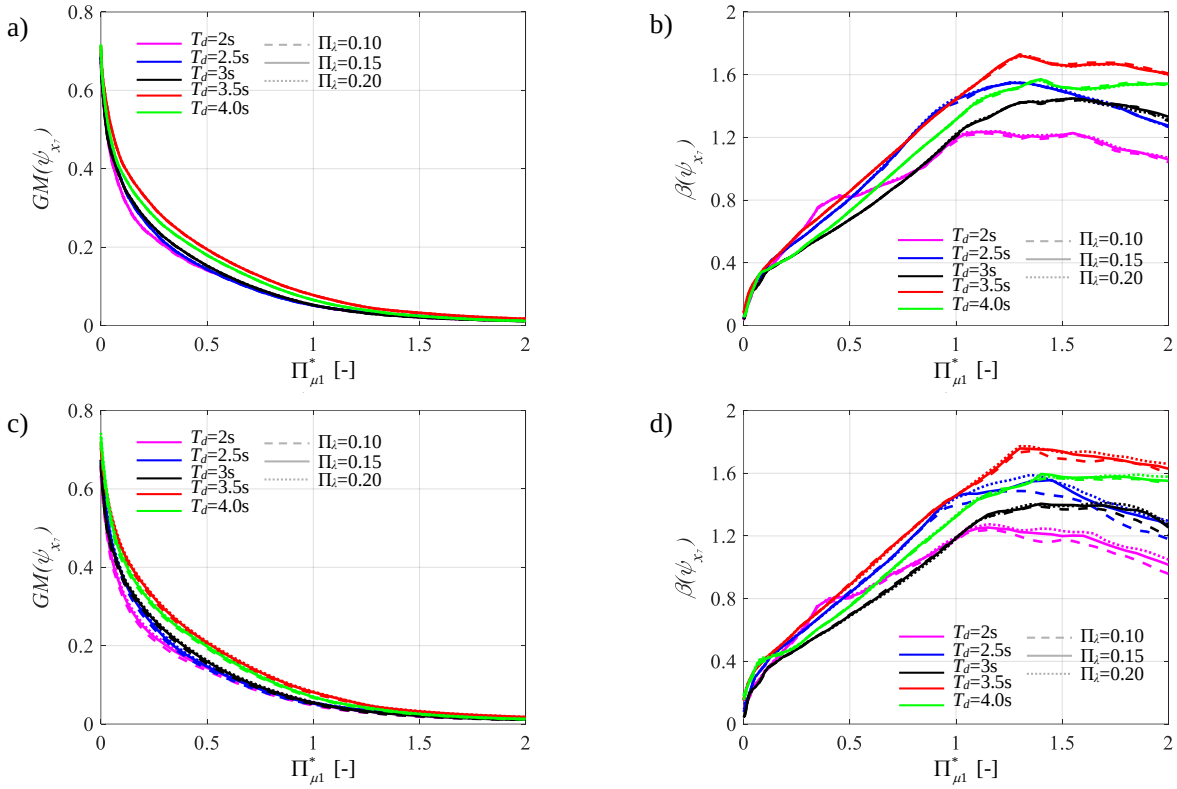

Figure 6. Normalized pier bearing response along the upper surface vs. $\Pi^*_{\mu 1}$: median value and dispersion for T_p = 0.1s (a and b) and T_p = 0.2s (c and d), for different values of Π_λ and T_d. Case 1.

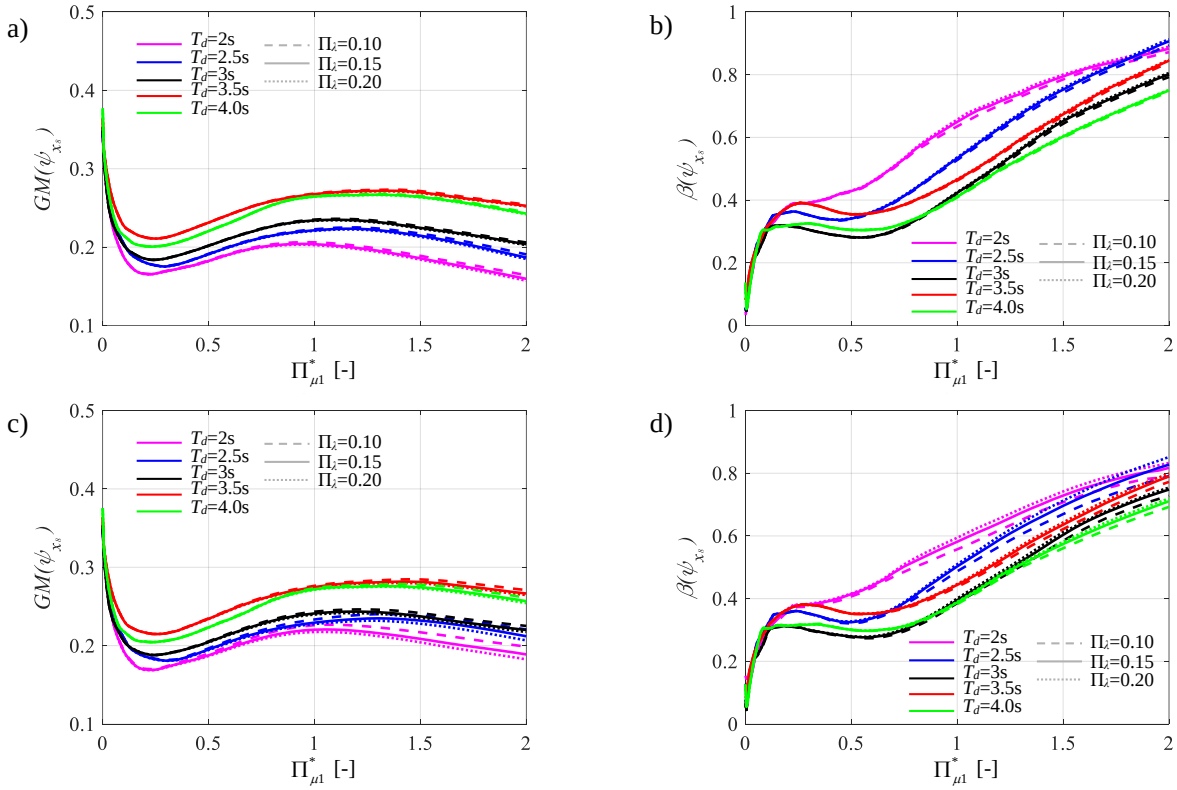

Figure 7. Normalized abutment bearing response along the lower surface vs. $\Pi^*_{\mu 1}$: median value and dispersion for T_p = 0.1s (a and b) and T_p = 0.2s (c and d), for different values of Π_λ and T_d. Case 1.

Within the case 1, Fig.s 7 (a) and (c) represent the geometric mean of the peak normalized response referring to the abutment bearing displacement along the lower surface (surface 2) $GM(\psi_{x_8})$, for T_p = 0.1s and T_p = 0.2s. This sliding surface is characterised by lower values of both radius of curvature and sliding friction coefficient (Table 1). These curves are in line with the ones referred to the peak response along the lower surface of the pier bearing (Fig.s 5 (a) and (c)). It

is possible to observe slightly lower values for $\Pi^*_{\mu 1}$ lower than 0.5, with a less marked influence of both T_p and Π_λ. Even the values of $\beta\left(\psi_{x_8}\right)$ are similar to those related to the lower surface of the pier bearing.

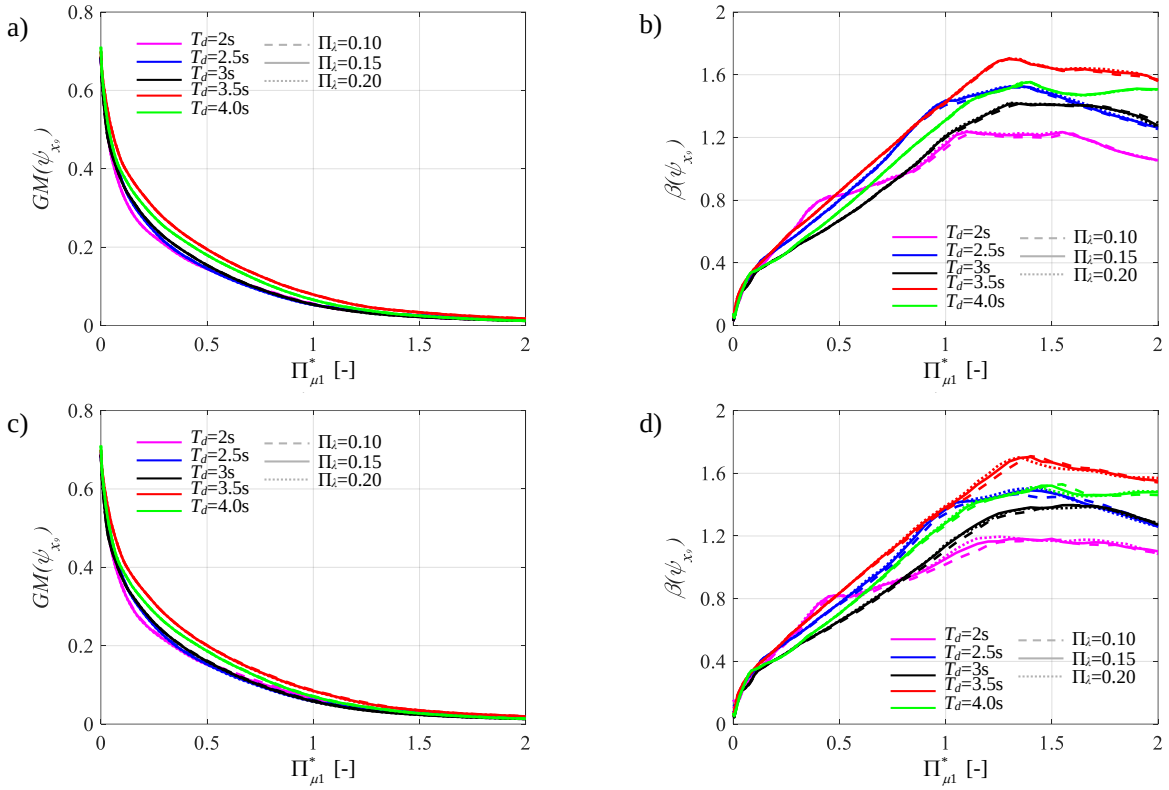

Figure 8. Normalized abutment bearing response along the upper surface vs. $\Pi^*_{\mu 1}$: median value and dispersion for T_p = 0.1s (a and b) and T_p = 0.2s (c and d), for different values of Π_λ and T_d. Case 1.

Fig.s 8 (a) and (c) show the variation with the system properties of the geometric mean of the peak normalized abutment bearing response along the upper surface (surface 1) $GM(\psi_{x_9})$, for T_p = 0.1s and T_p = 0.2s, in relation to the case 1. This sliding surface is characterised by higher values of both radius of curvature and sliding friction coefficient (Table 1). The results are once again strictly comparable with the ones of Fig.s 6 (a) and (c). Fig.s 8 (b) and (d) show the dispersion $\beta\left(\psi_{x_9}\right)$ assuming very low values for low $\Pi^*_{\mu 1}$ values, whereas it rises with rising values of $\Pi^*_{\mu 1}$. These values in Fig. 8 are slightly lower with respect to the ones in Fig. 6 with a less marked influence of both T_p and Π_λ.

Fig.s 6 and 8 demonstrate a higher influence of the upper surface (surface 1), characterized by higher values of the sliding friction coefficient and of the radius of curvature (Table 1), in representing the global response of the DCFP device at both the abutment and pier side as shown in Fig.s 3 and 4, especially, for $\Pi^*_{\mu 1}$ lower than 0.5. In fact, it is the upper surface that plays a crucial role for high intensities to elongate the isolated period and to dissipate more energy.

The existence of an optimal value of the normalised friction coefficient of the upper surface $\Pi^*_{\mu 1}$ for the both DCFP devices able to minimize the displacement of pier top (Fig. 2) is the result of counteracting effects that occur for increasing values of the friction coefficient as also highlighted in [40]-[41]: i) increase of the isolator strength with increase of the effective stiffness [66]-[67] and a consequential reduction of the corresponding effective fundamental vibration period [66]-[67]; ii) increase of the effects due to higher vibration modes as well as transfer of forces towards the superstructure; iii) increase of energy dissipation (equivalent damping).

Fig.s 9-12 represent the statistics of the main non-dimensional peak response parameters related to the case 2 of Table 1. Fig.s 9 (a) and (c), related to the geometric mean of the peak pier top displacement $GM(\psi_{u_p})$ and compared with Fig.s 2 (a) and (c) for the case 1, show a more marked increase against increasing $\Pi^*_{\mu 1}$ values as well as a more marked influence of all the structural properties. This is mainly related to a less efficiency of the isolation system as an higher friction coefficient at the lower surface (Table 1-case 2) leads to a general increase in μ_{eqv} (Eq.(5)) so that the corresponding increase in the secant stiffness moves the effective period towards larger pseudo-spectral acceleration values. Similarly to the case 1, there exists an optimal value of $\Pi^*_{\mu 1}$ such that the peak displacement of pier top is minimized. Fig.s 9 (b) and (d), with regard to the dispersion $\beta(\psi_{u_p})$, demonstrate a similarity with the dispersion values (Fig.s 2 (b) and (d)) of

the case 1, except when large values of $\Pi^*_{\mu 1}$ and low values of T_d are coupled together: there is an amplification because high friction coefficient values together with low isolation period values lead to an increase of the forces transmitted between the deck and the pier in the case 2.

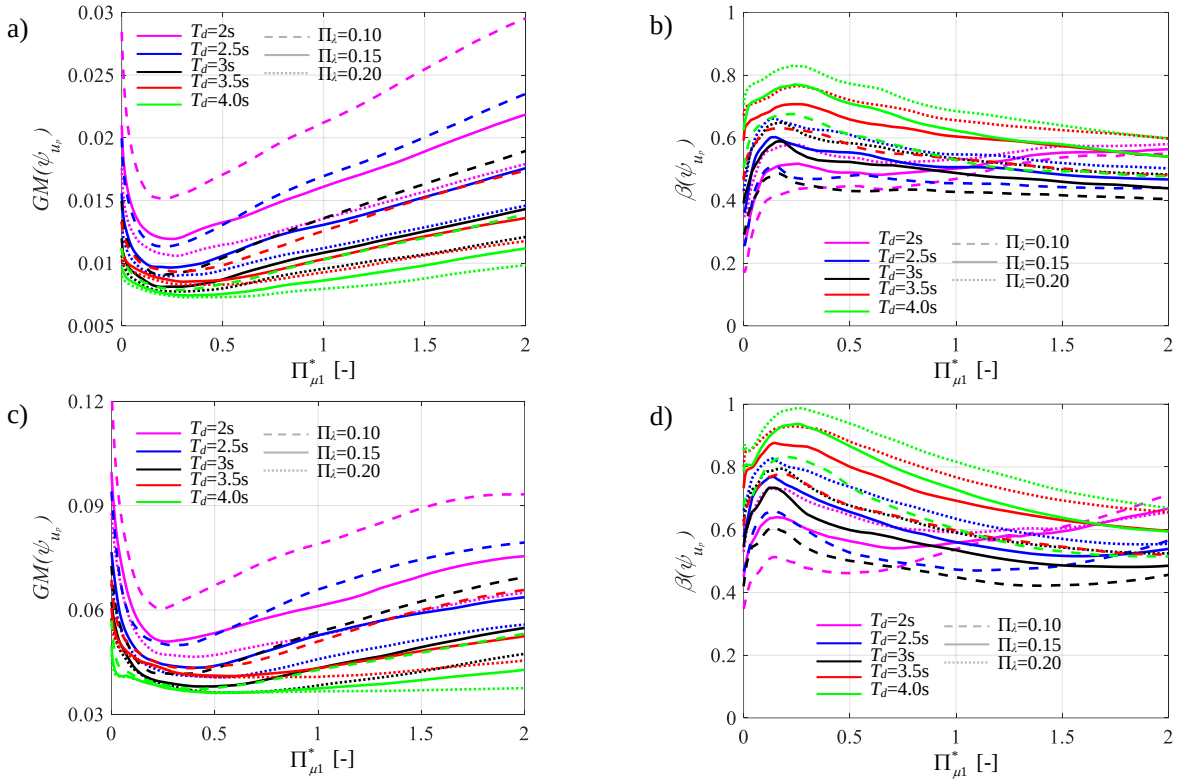

Figure 9. Normalized displacement of pier top vs. $\Pi^*_{\mu 1}$: median value and dispersion for T_p = 0.1s (a and b) and T_p = 0.2s (c and d), for different values of Π_λ and T_d. Case 2.

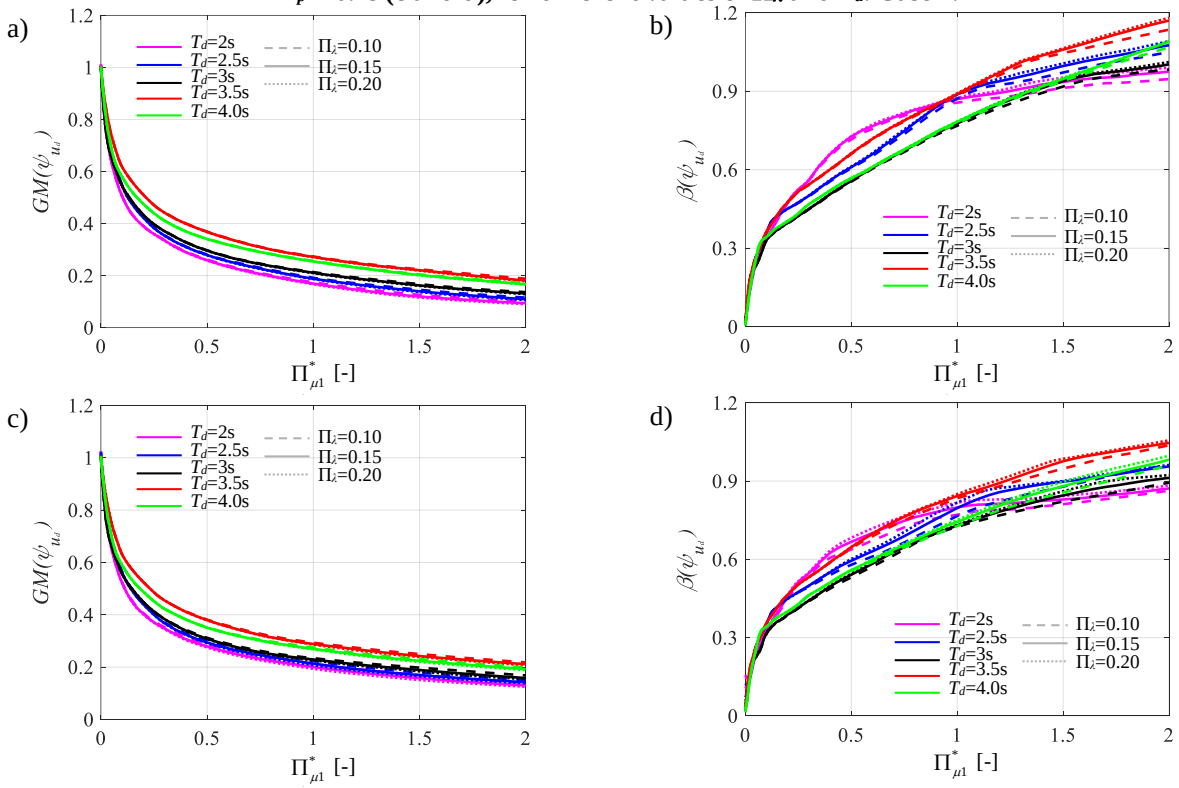

Figure 10. Normalized deck displacement vs. $\Pi^*_{\mu 1}$: median value and dispersion for T_p = 0.1s (a and b) and T_p = 0.2s (c and d), for different values of Π_λ and T_d. Case 2.

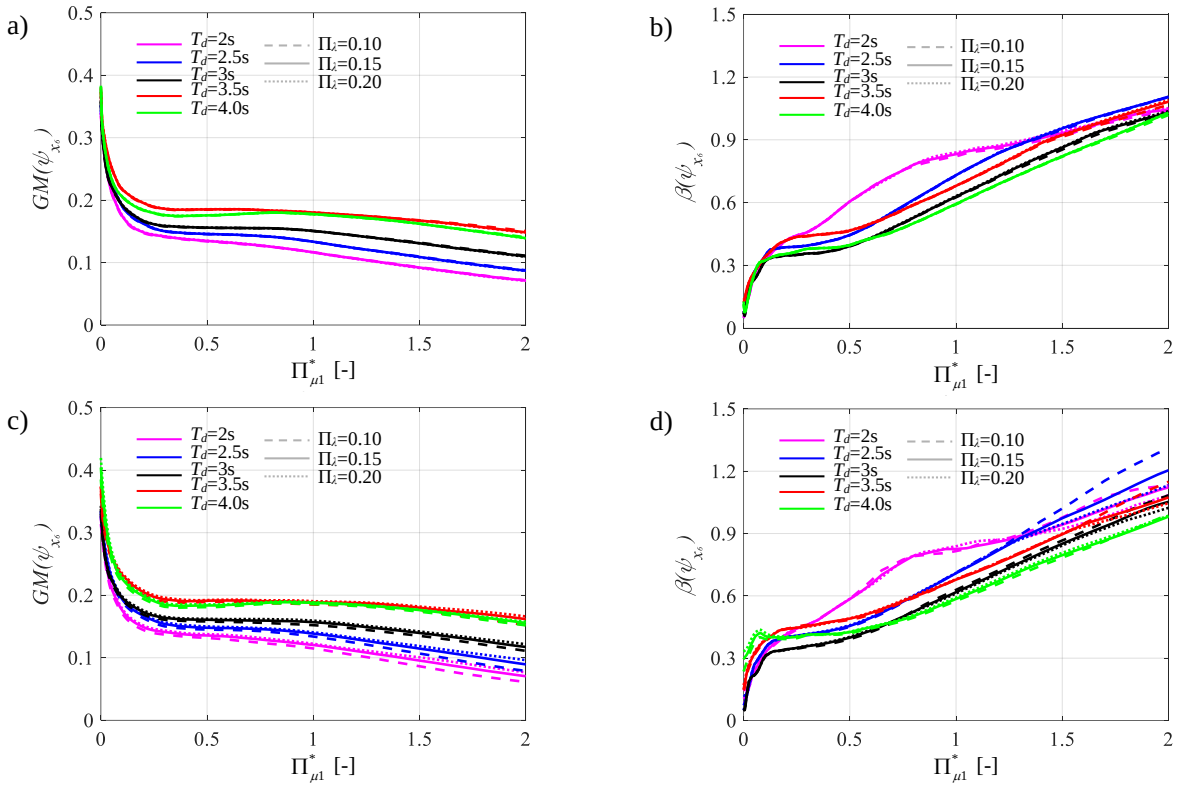

Figure 11. Normalized pier bearing response along the lower surface vs. $\Pi^*_{\mu 1}$: median value and dispersion for T_p = 0.1s (a and b) and T_p = 0.2s (c and d), for different values of Π_λ and T_d. Case 2.

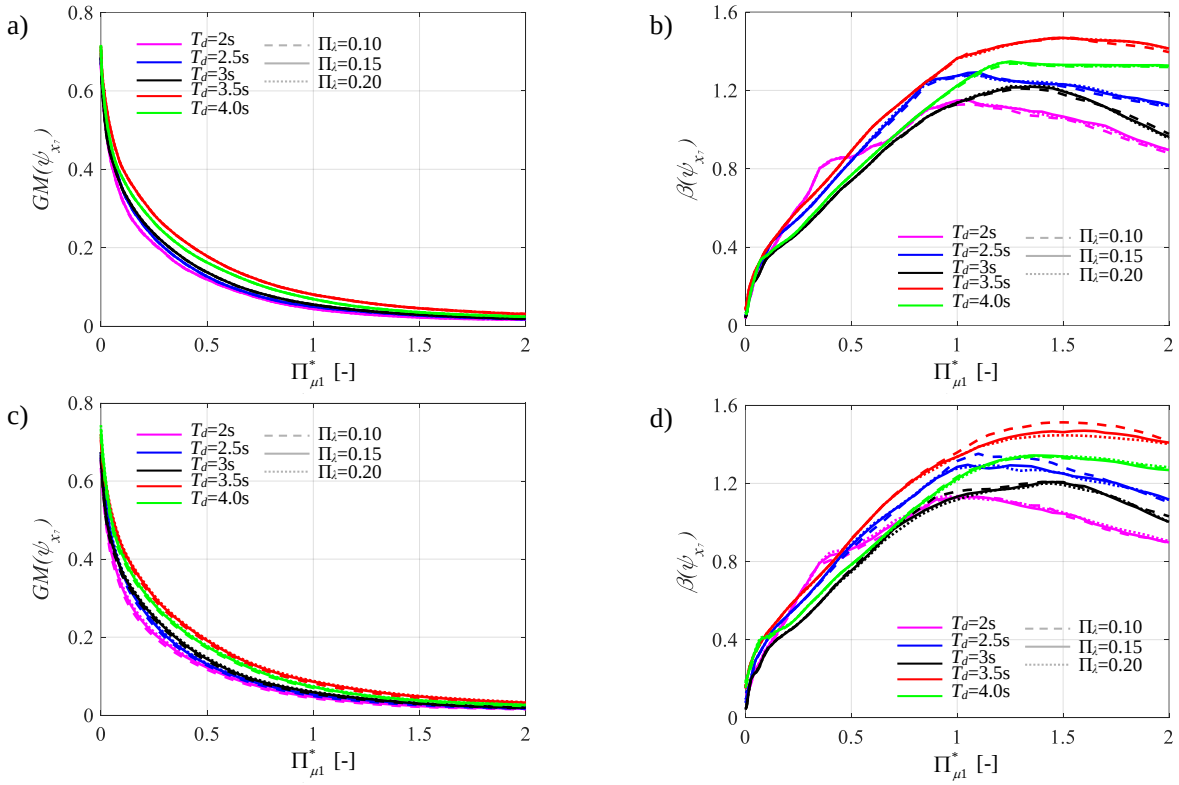

Figure 12. Normalized pier bearing response along the upper surface vs. $\Pi^*_{\mu 1}$: median value and dispersion for T_p = 0.1s (a and b) and T_p = 0.2s (c and d), for different values of Π_λ and T_d. Case 2.

Fig.s 10 (a) and (c) report the geometric mean of the peak global response of the bearing placed on the abutment $GM(\psi_{u_d})$ showing smaller values with respect to the case 1 (Fig.s 3 (a) and (c)), and this is consistent with the higher values of the friction coefficient along the lower surface that permit to reduce the maximum displacement of the DCFP bearing. With regard to the dispersion values $\beta(\psi_{u_d})$, Fig.s 10 (b) and (d) present values significantly larger than the case 1. Furthermore, the results have shown the same trend in terms of the geometric mean for the peak global response

of the bearing on the pier $GM(\psi_{x_d})$. In fact, $GM(\psi_{x_d})$ presents smaller values with respect to the ones reported for the case 1 as well as the dispersion values $\beta(\psi_{x_d})$ present higher values in the case 2.

Fig.s 11-12 depict, for the pier DCFP isolator, the peak response along the lower and the upper surface, respectively. With respect to the case 1, $GM(\psi_{x_6})$ presents lower values for increasing $\Pi^*_{\mu 1}$; $\beta(\psi_{x_6})$ presents higher values. Regarding the upper surface, $GM(\psi_{x_7})$ is very similar to the case 1 with slightly lower values; $\beta(\psi_{x_7})$ shows smaller values than the case 1. Furthermore, referring to the results of the peak response of the abutment bearing along the lower and upper surface, respectively: $GM(\psi_{x_8})$ has a trend similar with the one of the pier isolator $GM(\psi_{x_6})$ with slightly lower values; similarly for the $\beta(\psi_{x_8})$ with respect to $\beta(\psi_{x_6})$. Also $GM(\psi_{x_9})$ has a trend similar with the one of the pier isolator $GM(\psi_{x_7})$; $\beta(\psi_{x_9})$ presents slightly lower values with respect to $\beta(\psi_{x_7})$.

It is worth highlighting that all these normalized results, shown in Fig.s (2)-(12), can be expressed in dimensional terms using Eq.(14) and adopting $S_A(T_d)$ as a_0 (Section 4.1) according to a specific seismic ultimate limit state for a specific site. Moreover, through Eq.(17), both the 50th and 84th percentiles of the dimensional results can be computed. It follows that all the presented non-dimensional results are exploitable for the preliminary design or retrofit of multi-span continuous deck bridges, isolated with DCFP devices, located in any site and in relation, especially, to the seismic ultimate limit states. In fact, the response of the deck (i.e., global response of the isolators), of the pier and for each surface of the DCFP devices can be estimated. In addition, the in-plan radius for each surface of the isolator as well as the abutment-deck joints can be also defined.

OPTIMAL FRICTION COEFFICIENTS NORMALISED WITH RESPECT TO THE SEISMIC INTENSITY

Fig.s 13(a-b) illustrate the optimal values of the normalized friction coefficient $\Pi^*_{\mu 1,optimum}$ able to minimize the 50th and 84th percentiles of the seismic normalized demand to the pier ψ_{u_p}, for the case 1, with respect to Π_λ, T_p and T_d, in the range of $\Pi^*_{\mu 1}$ between 0 and 0.5. It is observed that $\Pi^*_{\mu 1,optimum}$ referred to the 50th percentile is not so variable only for $T_d = 2s$. For higher values, $\Pi^*_{\mu 1,optimum}$ generally increases with Π_λ and T_p. When high values of T_d are combined with low values of Π_λ and high values of T_p, $\Pi^*_{\mu 1,optimum}$ is low in order to reduce the isolator effective stiffness [66]-[67] and improve the effectiveness of the isolation technique.

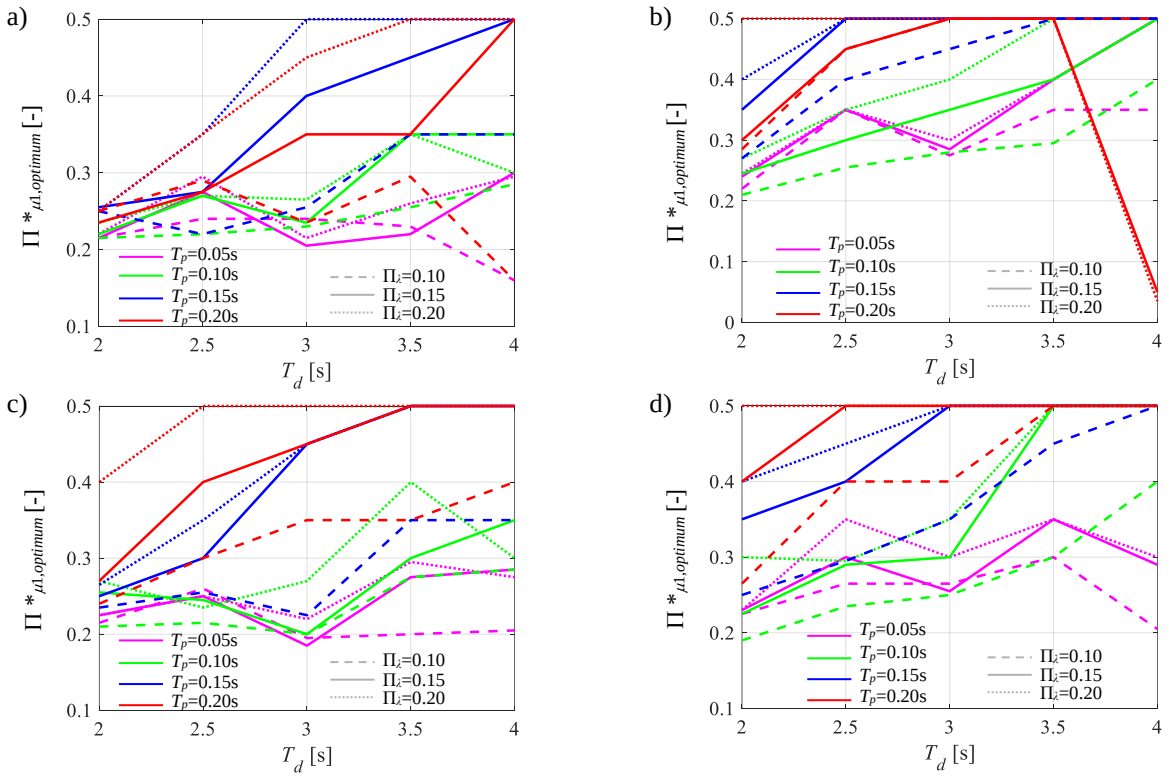

Figure 13. Optimal values of the normalized friction coefficient $\Pi^*_{\mu 1,optimum}$ vs. T_d; 50th (a,c) and 84th (b,d) percentiles; (a,b): case 1; (c,d): case 2.

Finally, the optimal values generally increase by increasing the percentile level. It is possible to reveal as the optimal friction corresponding to the 84th percentile tends to rise by increasing Π_λ, T_p and T_d. However, for some structural properties combination, lower $\Pi^*_{\mu 1,optimum}$ are required in order to reduce the isolator effective stiffness [66]-[67] and improve the effectiveness of the isolation technique. Fig.s 13(c-d) report the variation of $\Pi^*_{\mu 1,optimum}$, with respect to the same system properties for the case 2 of Table 1. As for the 50th percentile, $\Pi^*_{\mu 1,optimum}$ presents, in comparison with the case 1, a stronger regularity with all the three properties, having a monotonic rising, especially for $T_d = 3s; T_d = 3.5s; T_d = 4s$. A plateau is reached for $T_d = 3.5s$ and $T_d = 4s$ in correspondence of $T_p = 0.15s$ with a larger magnitude than the one seen in the case 1. This is due to the accumulated energy before that the surfaces slide due to a higher friction coefficient at the lower surface of the DCFP device. As for the 84th percentile, the case 2 outlines generally smaller values than the case 1.

According to Eq.(13) and adopting $S_A(T_d)$ as a_0 (Section 4.1) in line with a specific seismic ultimate limit state for a specific site, the optimal (non-normalised) friction coefficient of the upper surface (surface 1) can be easily calculated as $\mu_{1,\max,opt} = \Pi^*_{\mu 1,optimum} \cdot S_A(T_d)/g$. Thus, it increases linearly with the *IM* level. Successively, depending on the case of Table 1, it is possible to define the (non-normalised) value of the friction coefficient at the lower sliding surface (surface 2). These values, specific for any combination of the main dynamic properties of an isolated bridge, may be used for a preliminary either design or retrofit of a bridge in any site and in relation, especially, to the seismic ultimate limit states. If these optimal values are selected, the corresponding values of the relevant seismic response parameters for the deck (i.e., global response of the isolators), the pier and for each surface of the DCFP devices derive from the figures illustrated in the previous section as already commented. Similarly, the corresponding values of the in-plan radius for each surface of the isolator as well as of the abutment-deck joints can be defined.

It is also worth underlining that the proposed results have been achieved considering only the seismic loads, but during the design/verification phase of bridges, other serviceability actions such as thermal movements [68] have to be absolutely considered. These factors, in fact, can influence the design/retrofitting costs of piers and of foundations when high values of the friction coefficient are necessary under strong earthquake events. For these situations, a global cost-effectiveness analysis could be useful to reduce the costs provided that the same safety level is assured. Moreover, the deterioration of the sliding surface of the isolator can be taken into account by means of the property modification factors, as discussed in [69].

CONCLUSIONS

This paper analyzes the seismic performance of multi-span continuous deck bridges isolated with DCFP devices. Proposing a nondimensionalization of the motion equations with respect to the seismic intensity and specific for this system, the results of an extensive parametric study encompassing a wide range of isolator and bridge properties have been illustrated monitoring various response parameters of interest related to both the isolators and the pier. Specifically, the RC pier is considered elastic, whereas the RC deck and RC abutment are assumed rigid. Two cases corresponding to different ratios between the sliding friction coefficients of the DCFP device surfaces are investigated. Considering non-frequent ground motions, the results in terms of geometric mean and dispersion for each peak normalised response parameter are summarized as follows.

- Regarding the pier performance, there exists an optimal value of sliding friction coefficient for each surface of the DCFP device able to minimize the pier response. This optimal value depends on the bridge and isolator properties. As for the case 2, higher values are achieved since a higher friction coefficient at the lower surface leads to an increase in the isolator effective stiffness with a reduction of the isolation effective period and increase of the forces to the pier.
- Regarding the deck performance, which also corresponds to the peak global response of the bearing placed on the abutment, the response decreases significantly as the sliding friction coefficient increases. Slightly lower results are achieved for the global response of the bearing placed on the pier. As for the case 2, smaller values are obtained as higher friction coefficients along the lower surface permit to reduce the maximum displacement of the DCFP bearing.
- Regarding the surface 2 of the DCFP device on the pier, the peak normalized response decreases at first quickly, and then slightly increases for high values of the sliding friction coefficient. Slightly lower results are achieved for the lower surface (surface 2) of the DCFP device on the abutment. Within the case 2, lower response values are achieved.
- Regarding the surface 1 of the DCFP device on the pier, the peak normalized response hyperbolically decreases with increasing the sliding friction coefficient. Slightly lower values are achieved for the normalized response along the upper surface for the DCFP device on the abutment. Within the case 2, the results are very similar with the case 1.
- All the results show a higher influence of the upper surface, having higher values of the sliding friction coefficient and of the radius of curvature, in representing the global response of the DCFP devices at both the abutment and pier side. In fact, the upper surface is crucial at high intensities to elongate the isolated period and to dissipate more energy.

Then, optimal normalised friction coefficients aimed at minimizing the different percentiles (i.e., 50th and 84th) of the non-dimensional peak response of the pier are numerically computed, observing that the optimal value increases with the percentile, pier period and mass ratio. This trend is not always respected because for some structural properties

combinations, lower values of the optimal normalised friction coefficient are required to reduce the isolation effective stiffness and improve the effectiveness of the isolation. As for the case 2, lower values are generally achieved.
All the presented normalised results are useful for the preliminary design or retrofit of multi-span continuous deck bridges, isolated with DCFP devices, located in any site. In addition, they are effective, especially, in relation to the seismic ultimate limit states for the ground motions selected within the proposed non-dimensionalization with respect to the seismic intensity. In this way, knowing the dynamic properties of the bridge system, it is possible to evaluate, in non-dimensional form, the optimal properties of the seismic isolation combined with the corresponding seismic displacement demand to the different structural components at different percentiles (i.e., 50^{th} and 84^{th}). From these normalized values, it is possible to calculate the optimal (non-normalised) sliding friction coefficient for each surface of the seismic device and the dimensional bridge response parameters by means of linear relationships using the seismic intensity level in terms of $S_A(T_d)$ according to a specific seismic ultimate limit state for a specific site.

REFERENCES

[1] M. C. Constantinou, A. Kartoum, A. M. Reinhorn, P. Bradford , Sliding isolation system for bridges: Experimental study, *Earthquake Spectra* 1992; 8(3): 321-344.

[2] A. Kartoum, M. C. Constantinou, A. M. Reinhorn, Sliding isolation system for bridges: Analytical study, *J. Struct. Eng.* 1992; 8(3): 345-372.

[3] P. Tsopelas, M. C. Constantinou, Y. S. Kim, S. Okamota, Experimental study of FPS system in bridge seismic isolation, *Earthquake Eng. Struct. Dyn.* 1996; 25(1): 65-78.

[4] P. Tsopelas, M. C. Constantinou, S. Okamoto, S. Fujii, D. Ozaki, Experimental study of bridge seismic sliding isolation systems, *Eng. Struct.* 1996; 18(4): 301-310.

[5] A. Ghobarah, H. M. Ali, Seismic performance of highway bridges, *Eng. Struct.* 1988; 10(3): 157-166

[6] D. H. Turkington, A. J. Carr, N. Cooke, P. J. Moss, Seismic design of bridges on lead-rubber bearings, *J. Struct. Eng.* 1989; 115(12): 3000-3016.

[7] Jangid R. S., Seismic response of isolated bridges, *J. Bridge Eng.* 2004; 9(2): 156-166.

[8] Jangid, R. S. (2008). Equivalent linear stochastic seismic response of isolated bridges. *Journal of Sound and Vibration*, 309(3-5), 805-822.

[9] N.P. Tongaonkar, R.S. Jangid. Seismic response of isolated bridges with soil–structure interaction. *Soil Dynamics and Earthquake Engineering* 23 (2003) 287–302.

[10] Olmos, B. A., Jara, J. M., & Roesset, J. M. (2011). Effects of isolation on the seismic response of bridges designed for two different soil types. Bulletin of Earthquake Engineering, 9(2), 641-656.

[11] R. S. Jangid, Stochastic Response of Bridges Seismically Isolated by Friction Pendulum System, *J. Bridge Eng*. 2008; 13(4): (319).

[12] R. S. Jangid, Optimum friction pendulum system for near-fault motions. *Engin. Structures* 2005; 27(3): 349–359.

[13] Dicleli, M., & Buddaram, S. (2006). Effect of isolator and ground motion characteristics on the performance of seismic-isolated bridges. Earthquake engineering & structural dynamics, 35(2), 233-250.

[14] Y. P. Wang, L. L. Chung, W. H. Liao, Seismic response analysis of bridges isolated with friction pendulum bearings, *Earthquake Eng. Struct. Dyn.* 1998; 27(10): 1069-1093.

[15] Kunde, M. C., & Jangid, R. S. (2006). Effects of pier and deck flexibility on the seismic response of isolated bridges. Journal of Bridge Engineering, 11(1), 109-121.

[16] Mitoulis, S. A. (2012). Seismic design of bridges with the participation of seat-type abutments. Engineering Structures, 44, 222-233.

[17] Mitoulis, S. A., Palaiochorinou, A., Georgiadis, I., & Argyroudis, S. (2016). Extending the application of integral frame abutment bridges in earthquake-prone areas by using novel isolators of recycled materials. Earthquake Engineering & Structural Dynamics, 45(14), 2283-2301.

[18] Zhang, J., & Makris, N. (2002). Seismic response analysis of highway overcrossings including soil–structure interaction. Earthquake engineering & structural dynamics, 31(11), 1967-1991.

[19] Zhang, J., & Makris, N. (2002). Kinematic response functions and dynamic stiffnesses of bridge embankments. Earthquake engineering & structural dynamics, 31(11), 1933-1966.

[20] VA. Zayas, SS. Low, SA. Mahin, A simple pendulum technique for achieving seismic isolation. *Earthquake Spectra* 1990; 6:317–33.

[21] L. Su, G. Ahmadi , IG. Tadjbakhsh, Comparative study of base isolation systems. *Journal of Engineering Mechanic* 1989; 115:1976–92.

[22] A. Mokha , MC. Constantinou, AM. Reinhorn, Teflon Bearings in Base Isolation. I: Testing. *J. Struct. Eng.* 1990; 116(2): 438-454.

[23] M. C. Constantinou, A. Mokha, A. M. Reinhorn, Teflon Bearings in Base Isolation. II: Modeling. *J. Struct. Eng*. 1990; 116(2):455-474.

[24] M. C. Constantinou, AS. Whittaker, Y. Kalpakidis, DM. Fenz, GP. Warn, Performance of Seismic Isolation Hardware Under Service and Seismic Loading. Technical Report, 2007.

[25] J. L. Almazàn, J. C. De la Llera, Physical model for dynamic analysis of structures with FPS isolators. *Earthquake Engineering and Structural Dynamics* 2003; 32:1157–1184.

[26] Murat Eröz, Reginald DesRoches. Bridge seismic response as a function of the Friction Pendulum System (FPS) modeling assumptions. *Eng. Str.*, 2008, 30: 3204–3212.

[27] Eröz, M., & DesRoches, R. (2013). The influence of design parameters on the response of bridges seismically isolated with the friction pendulum system (FPS). Engineering structures, 56, 585-599.

[28] D. M. Fenz, M. C. Constantinou, Behaviour of the double concave friction pendulum bearing, *Earthquake Engineering and Structural Dynamics*, 2006; 35:1403-1424.

[29] M. C. Constantinou, Friction pendulum double concave bearings, technical report. University of Buffalo NY, October 29, 2004.

[30] Y. S. Kim, C. B. Yun, Seismic response characteristics of bridges using double concave friction pendulum bearings with tri-linear behavior. *Engin. Struct*. 29, 2007, 3082-3093.

[31] Masoud Malekzadeh, Touraj Taghikhany. Multi-Stage Performance of Seismically Isolated Bridge Using Triple Pendulum Bearings. *Advances in Str. Engineering* Vol. 15 No. 7, 2012.

[32] P. Castaldo, M. Ripani, R. Lo Piore, Influence of soil conditions on the optimal sliding friction coefficient for isolated bridges, *Soil Dynamics and Earthquake Engineering*, 2018, 111; 131–148.

[33] Zhang, J., & Huo, Y. (2009). Evaluating effectiveness and optimum design of isolation devices for highway bridges using the fragility function method. Engineering Structures, 31(8), 1648-1660.

[34] P. Castaldo, B. Palazzo, P. Della Vecchia, Life-cycle cost and seismic reliability analysis of 3D systems equipped with FPS for different isolation degrees, *Engineering Structures*, 2016; 125: 349–363.

[35] P. Castaldo, B. Palazzo, T. Ferrentino T., Seismic reliability-based ductility demand evaluation for inelastic base-isolated structures with friction pendulum devices, *Earthquake Engineering and Structural Dynamics*, 2017, 46(8): 1245-1266, DOI: 10.1002/eqe.2854.

[36] P. Castaldo, G. Alfano, Seismic reliability-based design of hardening and softening structures isolated by double concave sliding devices, *Soil Dynamics and Earthquake Engineering*, 129: 105930, 2020.

[37] P. Castaldo, B. Palazzo, G. Alfano, MF. Palumbo, Seismic reliability-based ductility demand for hardening and softening structures isolated by friction pendulum bearings, 2018, *Struc. Control and Health Monitoring*, e2256.

[38] P. Castaldo, G. Amendola, B. Palazzo, Seismic fragility and reliability of structures isolated by friction pendulum devices: Seismic reliability-based design (SRBD), *Earth. Engin. and Struct. Dyn.*, 2017, 46(3); 425–446.

[39] E. Tubaldi E, L. Ragni, A. Dall'Asta, Probabilistic seismic response assessment of linear systems equipped with nonlinear viscous dampers, *Earthquake Engineering & Structural Dynamics* 2014; DOI: 10.1002/eqe.2461.

[40] P. Castaldo, E. Tubaldi, Influence of FPS bearing properties on the seismic performance of base-isolated structures, *Earthquake Engineering & Structural Dynamics*, 2015; 44(15): 2817-2836.

[41] P. Castaldo, E. Tubaldi, Influence of ground motion characteristics on the optimal single concave sliding bearing properties for base-isolated structures. *Soil Dynamics and Earthquake Engineering*, 2018, 104: 346–364.

[42] NTC18. Norme tecniche per le costruzioni. Gazzetta Ufficiale del 20.02.18, DM 17.01.18, Ministero delle Infrastrutture.

[43] NCEER-94-0002 "NCEER-Taisei Corporation Research Program on Sliding Seismic Isolation Systems for Bridges: Experimental and Analytical Study of Systems Consisting of Sliding Bearings, Rubber Restoring Force Devices and Fluid Dampers," Volumes I and II, by P. Tsopelas, S. Okamoto, M.C. Constantinou, D. Ozaki and S. Fujii, 2/4/94, (PB94-181740, A09, MF-A02 and PB94-181757, A12, MF-A03).

[44] M.C. Constantinou,.; I. Kalpakidis, A. Filiatrault and R.A. Ecker Lay, LRFD-Based Analysis and Design Procedures for Bridge Bearings and Seismic IsolatorsMCEER-11-0004

[45] Priestley MJN, Seible F, Calvi GM. Seismic design and retrofit of bridges. Wiley; 1996.

[46] RD. Bertero, VV. Bertero, Performance-based seismic engineering: the need for a reliable conceptual comprehensive approach. *Earthquake Engineering and Structural Dynamics*, 2002; 31:627–652.

[47] H. Aslani, E. Miranda, Probability-based seismic response analysis. *Engin. Structures* 2005; **27**(8): 1151-1163.

[48] N. Shome, C. A. Cornell, P. Bazzurro, J. E. Carballo, Earthquake, records, and nonlinear responses. *Earthquake Spectra*, 1998, 14(3); 469-500.

[49] N. Luco, C. A. Cornell, Structure-specific scalar intensity measures for near-sorce and ordinary earthquake ground motions. *Earthquake Spectra*, 2007, 23(2); 357-392.

[50] Baker, J. W., & Lee, C. (2018). An improved algorithm for selecting ground motions to match a conditional spectrum. Journal of Earthquake Engineering, 22(4), 708-723.

[51] Kitayama, S., & Constantinou, M. C. (2018). Collapse performance of seismically isolated buildings designed by the procedures of ASCE/SEI 7. Engineering Structures, 164, 243-258.

[52] Baker, J. W. (2011). Conditional mean spectrum: Tool for ground-motion selection. Journal of Structural Engineering, 137(3), 322-331.

[53] Lin, T., Haselton, C. B., & Baker, J. W. (2013). Conditional spectrum-based ground motion selection. Part I: hazard consistency for risk-based assessments. Earthquake engineering & structural dynamics, 42(12), 1847-1865.

[54] Kitayama, S., & Constantinou, M. C. (2019). Effect of displacement restraint on the collapse performance of seismically isolated buildings. Bulletin of Earthquake Engineering, 17(5), 2767-2786.

[55] Kitayama, S., & Constantinou, M. C. (2019). Probabilistic seismic performance assessment of seismically isolated buildings designed by the procedures of ASCE/SEI 7 and other enhanced criteria. Engine. Struct., 179, 566-582.

[56] ATC-63. Quantification of building seismic performance factors. FEMAP695. Redwood City, CA, 2008.

[57] K. Ryan, A. Chopra, Estimation of Seismic Demands on Isolators Based on Nonlinear Analysis. *Journal of Structural Engineering* 2004; 130(3): 392–402.

[58] E. Tubaldi, L. Ragni, A. Dall'Asta, Probabilistic seismic response assessment of linear systems equipped with nonlinear viscous dampers, *Earthquake Engineering & Structural Dynamics* 2014; DOI: 10.1002/eqe.2461.

[59] C. A. Cornell C, F. Jalayer, R. Hamburger, D. Foutch, Probabilistic Basis for 2000 SAC Federal Emergency Management Agency Steel Moment Frame Guidelines. *Journal of Structural Engin.* 2002; 128(4): 526-533.

[60] A. H. S. Ang, W. H. Tang, Probability Concepts in Engineering-Emphasis on Applications to Civil and Environmental Engineering. John Wiley & Sons, New York, USA, 2007.

[61] Math Works Inc. MATLAB-High Performance Numeric Computation and Visualization Software. User's Guide. Natick: MA, USA, 1997.

[62] Yen-Po Wang, Lap-Loi Chung, Wei-Hsin Liao. Seismic response analysis of bridges isolated with friction pendulum bearings. *Earth.Eng.& Str. Dyn.*, 1998; 27, 1069-1093.

[63] M.C. Kunde, R.S. Jangid. Seismic behavior of isolated bridges: A-state-of-the-art review. *Electronic Journal of Structural Engineering*, 3 (2003).

[64] Evan m. Lapointe. An investigation of the principles and practices of seismic isolation in bridge structures. *Department of Civil and Environmental Engineering*; 2004.

[65] Michael D. Symans, Steven W. Kelly. Fuzzy logic control of bridge structures using intelligent semi-active seismic isolation systems. *Earth. Engng. Struct. Dyn.*, 28, 37-60, (1999).

[66] KM. Kelly, *Earthquake-Resistant Design with Rubber*. 2nd ed. Berlin and New York: Springer-Verlag; 1997.

[67] Building Seismic Safety Council. NEHRP Recommended Provisions: Design Examples FEMA 451 - Washington, D.C., August 2006.

[68] National cooperative highway research program report 276 - Thermal effects in concrete bridge superstructures, 1985.

[69] Warn Gordon P. and Andrew S. Whittaker, Property Modification Factors for Seismically Isolated Bridges, 2006, 11:3(371), 1084-0702.